Summary

The authors appreciate the many detailed suggestions, which were incorporated into the revised manuscript. The revised manuscript includes refined figures, less redundant information, and references to hydrological studies that highlight the importance of the study to the hydrology and earth system science community. Some sections of the original manuscript have been entirely deleted. The deleted sections are those examining the auto-bicoherence of Indian rainfall and the event decomposition of time series. The abstract and the first two paragraphs of the introduction section have been rewritten to better reflect the readership of the journal. The revised manuscript also includes an URL at the end of the discussion section to direct the reader to the computer software associated with the adopted methodology. More detailed responses to comments are provided below. The reviewer comments are in bold text and our responses to the comments are in plain text.

Reviewer 1

The purpose of this paper is to apply novel methods for bivariate, nonlinear wavelet analysis to understand whether apparent changes in the relationship between indices for ENSO and the Indian Monsoon represent fundamental changes in their relationship. The methods are based on those published in previous peer-reviewed papers by the authors, and so this paper can be viewed as an application of these methods to a relevant and interesting scientific problem. These tools for higher-order wavelet analysis allow the authors to quantify the nonlinearity of ENSO and indices for the Indian monsoon. The authors conclude from this analysis that ENSO nonlinearity is related to ENSO flavors, and that the apparent changes in the relationship between ENSO and Indian rainfall are also related to ENSO flavors. Finally, the authors use these findings to re-interpret findings by Yun and Timmerman (2018) which suggest that the breakdown of the ENSO-India rainfall relationship is related to shifts in the linearity of the ENSO regime. Specifically, the authors argue that the nonlinear relationship identified by their higher-order wavelet model will have non-Gaussian noise components, potentially confounding the alternative analysis. While this paper is unlikely to be the final word on this debate, it is a clear, well-written, and important contribution to the study of the ENSO-Indian rainfall relationship, and to time series analysis more broadly, and should be published pending minor stylistic edits. I also note a lack of a data availability policy [https://www.natural-hazards-and-earthsystem-sciences.net/about/data_policy.html]. Making the code and data used to others would help other researchers apply these methods to other time series.

A URL to the first author's website where the computer software for the adopted methodology can be obtained is provided Page 12 of the revised manuscript.

L9: It took me a while to understand the similarities and differences between the terms auto-bicoherence, bicoherence, coherence, etc. The auto-bicoherence is defined later, but perhaps a simple table or sentence near the introduction explaining the difference between these different terms would be helpful. (I am flagging this in the abstract but the clarification could happen elsewhere)

To better distinguish coherence traditionally used from the new methods, traditional coherence is now referred to as "linear coherence" in the revised abstract. Furthermore, a sentence mentioning how auto-bicoherence detects quadratic nonlinearities in time series has been added to the main text on Page 4 Line 174. The type of nonlinearities (e.g. cubic nonlinearities) that cannot be detected by the methods is mentioned on Page 5 Line 185. A table (Table 1 in revised manuscript) was added to clarify the nomenclature used in the paper.

L48: consider rephrasing "investigators"

"investigators" was changed to "researchers" in the revised manuscript.

L58-59: there are also concerns about data quality – would be worth at least referencing or discussing them https://www.natural-hazards-and-earth-system-sciences.net/about/data_policy.html

A careful literature search did not reveal any studies citing data quality issues regarding the All-India rainfall (AIR) data set. Nevertheless, as a gauge-based product, AIR has both the advantages and disadvantages of any product based on in situ weather stations—that is, the data that go into it are collected in a well-understood way, without use of proxies, but there is the potential for non-representative station distribution or faulty gauges. That said, AIR is widely used product that has been applied successfully to many studies of weather and climate in India.

L95 and beyond: please consider converting from month−1 to year−1

After careful consideration, we decided that we will still use months in the revised manuscript because of months seems to work better with how the wavelet scales and periods are calculated using powers of 2.

L117: are there possible data quality issues with the rainfall data?

To the authors knowledge, there are no serious data quality issues. The All-India rainfall data is frequently used in Indian Monsoon studies. Because of the importance of the Indian monsoon, careful data collection has been conducted since the 1800's.

L135: the formatting here has changed.

Thank you for identifying the formatting change. It was corrected in the revised manuscript.

L146: are there cases where very small events (say a single month) emerge? If so how are these handled?

To make the manuscript more concise, the event decomposition approach will be removed from the manuscript. Nevertheless, the single-month events were considered to be short events whose intensities were the values of the data points composing the events.

L156: Consider re-wording to continuous wavelet transform of a time series X = ... as a function of wavelet scale s is given by

The authors appreciate the suggestion for rewording the sentence. The sentence was recorded in the revised manuscript (Page 3, Line 136 of revised manuscript).

L160: if this transform is commonly used please cite. Are results sensitive to choice of wavelet form or to choice of ω?

The Morlet wavelet is the most commonly used analyzing wavelet in climate and hydrological studies because it balances time and frequency localization. A citation was added to indicate the common use of the Morlet wavelet on Page 4 Line 142. The choice of ω would impact the results given that it alters the time and frequency localization behavior of the Morlet wavelet. However, given that $\omega = 6$ is such a common choice in wavelet applications, the authors feel that it is beyond the scope of the paper to understand its effect on the interpretability of wavelet analysis results.

L188: it would help to be clearer here about what sorts of nonlinearities this analysis can pick up, which sorts of nonlinearities it cannot pick up, and what sorts of nonlinearities have been hypothesized or observed in ENSO time series.

We agree that a clarification is needed. In the revised manuscript, we now mention that the bicoherence method detects quadratic type nonlinearities on on Page 4 Line 174.

L200: see above comment regarding distinction between coherence, auto-coherence, etc.

A table (Table 1) was added to the revised manuscript to clarify the nomenclature used in the paper.

L464: if there are spatial shifts happening that are related to ENSO, this could potentially complicate some of this analysis correct?

While we agree that spatial patterns could be shifting, the purpose of the analysis was to quantify the auto-bicoherence of SSTs at various grid points. An additional study would be needed to see if there are spatial shifts in the patterns, which is beyond the scope of the paper.

L545: Consider re-wording "despite how"

"Despite how" was changed to "Although" in the revised manuscript on Page 10, Line 413 of revised manuscript.

L595: what is your interpretation of the finding that the modes found are not harmonics of 12 months? Given that the seasonal (12 month) cycle is important here and many of the other modes may be coupled to it, it would be useful to explain to the reader why other modes emerge as important.

Although understanding the specific dynamics underlying the nonlinear modes is beyond the scope of paper, the revised manuscript includes references to studies that focused on understanding nonlinear ENSO dynamics (Page 2, Line 76).

L610: this is an important point which the authors should consider emphasizing in the abstract

The authors agree that it is important point. As such, the finding will be discussed in the revised abstract.

Figure 5: consider adding color

We agree that this figure could be clearer. We thickened lines and changed the line color to red and blue shades designed to be distinguishable by the colorblind.

Figure 6: consider plotting the global (average) wavelet spectrum adjacent

Although the authors agree that the global wavelet power spectra would help highlight the dominant peaks in the wavelet power spectra, we could not find any reason to discuss them in the text because we are concerned with changes in wavelet power. For the sake of brevity, we decided to omit them.

Figure 7: please fix titles

Thank you for referring us to the errors in the titles. The problem was corrected in the revised manuscript.

Figure 8: the figure has gotten clipped at the left margin.

Thank you for referring us to the clipping problem. The problem was corrected in the revised manuscript.

Figure 9: this is the wrong place to bring this up but it would be helpful to add some discussion in the methods section, specifically around hypothesis testing, about what the 5% cumulative area-wise significance means and how to interpret it.

The authors agree that some discussion is warranted given the novelty of the statistical tests. A short discussion was added on Page 4, Line 207 of the revised manuscript, but the reader is referred to Schulte (2019) for more details.

Figure 11: please clarify why these pairs were chosen

As stated on Line 481, the pairs were chosen because they are local maxima in auto-bicoherence that are statistically significant. Choosing local maxima allows the spatial patterns shown in Figure 11 to emerge more clearly. A sentence clarifying our choice of pairs was inserted into the revised manuscript on Page 11, Line 466.

References

Schulte, J. A.: Statistical hypothesis testing in wavelet analysis: theoretical developments and applications to Indian rainfall, Nonlin. Processes Geophys., 26, 91-108, https://doi.org/10.5194/npg-26-91-2019, 2019.

Yun, Kyung-Sook and Axel Timmermann (2018). "Decadal Monsoon-ENSO Relationships Reexamined". Geophysical Research Letters 45.4. doi: 10.1002/2017GL076912.

GENERAL COMMENTS The manuscript investigates the relationship between rainfall and ENSO index using wavelet analysis and a wavelet coherence method is proposed to explain the changes of temporal correlation between two time series. The topic of the study is interesting may be outside the scope of the journal. This appears more so as almost all references are from climate journals where this paper sits more naturally. I think this paper should be withdrawn and submitted to an appropriate climate journal, or else reformatted to represent better arguments as to why it is of interest to hydrology directly. I have, however, read through the paper and have some comments that may help the authors publish this successfully.

Our manuscript addresses precipitation variability in the South Asian monsoon region. As precipitation in this region is critical to mountain glaciers, transboundary rivers, groundwater recharge, and functioning of many ecosystems and human systems, we believe that the topic is of considerable importance to hydrologists and Earth system scientists. However, we appreciate the reviewer's concern, and we recognize that we did not sufficiently emphasize the hydrological relevance of this work in the original manuscript. The first two paragraphs of the introduction section have been rewritten in the revised manuscript to better empathize the hydrological relevance. Many new references have been added as well.

COMMENT1: Section 2, the way authors computed the monthly anomaly by subtracting the data from the whole period is not the recommended and standard way. It is recommended by WMO that a fixed reference period is defined as the 30-year period 1 January 1961 to 31 December 1990. Authors should consider use this as baseline period, especially when compared SST and Nino indices over different regions.

Although the authors agree that a 30-year base period is commonly used in climate studies, it is unclear how using the standard base period would benefit the present analysis. Using a different base period would only translate the time series up or down uniformly and would not alter the actual behavior of the time series. Therefore, the results of the wavelet analysis, which are the focus of the present study, would be unchanged. Furthermore, skewness would be made relative to that base period, which would make the more recent skewed events appear less prominent. As such, we feel that subtracting the long-term means to calculate anomalies is the best approach for the present study. By using long-term means, it is easier to see how skewness how evolved throughout the study period, which is consistent with what the wavelet analysis is quantifying.

COMMENT2: Section 3.1, there is no such Reference Schulte and Lee (2019). More importantly, the reason of adapting Event Decomposition is not well explained and how it helps quantifying the nonlinearity (i.e. skewness) of rainfall and ENSO index is not demonstrated. In the end of Method section, authors considered a synthetic example to illustrate the concept of nonlinear coherence using original time series but following your methodology it should be transformed to event spectra before calculating the coherence. The impact of Event Decomposition on the wavelet analysis and coherency is unknown.

The authors agree that it is unclear how the event spectra benefit the paper. As such, the event decomposition method results have been removed from the revised manuscript. This removal allowed us to focus more on wavelet analysis, which is the main topic of the paper. The authors note that the coherence spectra are based on the actual time series and not on the event transformed time series.

COMMENT3: Section 4.2, the relation between skewness and correlation is not explicitly demonstrated. There is a sharp decrease of skewness of June-September rainfall around 1991. Is there any particular reason? And what is the implication of this change? "A comparison of Figures 5a and Figures 5c reveals that the weakening and reversal of the relationship occurs during the time period when the Niño 1+2 index is especially skewed, suggesting that ENSO skewness changes could be contributing to changes in the time-domain correlation between ENSO and All-India rainfall. " This conclusion is in doubt, Figure 5a doesn't include the skewness of August-September rainfall.

The main reason for showing skewness is because two time series can only be perfectly correlated if all the statistical moments are correlated. More specifically, if the skewness of one time series is increasing but another remains nearly constant, then the lack of correlation between the skewness of the two time series must be contributing to changes in the correlation between the time series. This idea was made more explicit in the revised manuscript (Page 6, Line

229). The sharp decrease in skewness around 1991 could be noise. A full understanding of all sources of Indian rainfall skewness would require additional analyses, which would digress from the focus of the paper, which is to relate ENSO skewness to Indian rainfall skewness. Nevertheless, an implication of the result is that noise also influences the correlation between Indian rainfall and ENSO. This possibility was mentioned in the revised manuscript on Page 9 Line 351.

COMMENT4: Section 4.2 and 4.3, through the global and local auto-bicoherence analysis, they show the nonlinearity of ENSO indices and India rainfall in the frequency and spatial space individually. But how these two related to each other, authors do not explain explicitly.

The main reasons for showing the local and global bicoherence analyses is to highlight their differences. Because the nonlinear coherence between them is weak, we expected that the differences to be large. On page 12, Line 496 of the revised manuscript, we mentioned how changing ENSO nonlinearity could explain the more frequency occurrence of Central Pacific El Nino in recent decades, connecting the spatial pattern of auto-bicoherence to local auto-bicoherence.

Using the nonlinear wavelet coherence method to test your hypothesis should be the major contribution of your work, however it is only briefly discussed in the very end of Section 4.3.2. There are lots of redundant information in the manuscript, which makes the paper long and difficult to read.

In the revised manuscript, we expanded the nonlinear wavelet coherence method section. In addition, some text was moved or deleted (e. g Section 4.2.2) of original manuscript) so that the nonlinear coherence section appears earlier in the revised manuscript. The authors agree that there is a lot of redundant information, which was reduced in the revised manuscript by deleting text (e. g Section 4.2.2 of original manuscript) and moving some information to the supplementary material. For example., Section 4.2.1 of the original manuscript is now the final section of the revised manuscript. We also now only focus on the All-India time series because looking at different regions of India is not necessary to get our key message across.

SPECIFIC POINTS:

1. EL Nino or El Nino, please keep it consistent throughout the paper.

The authors appreciate the identification of this inconsistency, which was corrected throughout the paper. The format was changed to "El Nino" throughout.

2. Line 104, keep the numbering format consistent.

The numbering inconsistency was corrected in the revised manuscript.

3. Please have a careful look of the format of your references.

The authors appreciate the comment about the reference formatting. The reference formatting was corrected in the revised manuscript.

4. Line 274, keep the equation numbering format consistent.

The equation formatting inconsistency was corrected in the revised manuscript.

5: Line 175, Because theory supports a casual link...Authors do not explain this point well. Does strong coherence or association mean causality in nonlinear system? More details are needed.

Authors agree that more details are needed regarding the causal linkage statement. There are many studies that have linked ENSO to the Indian monsoon. The Ropelewski and Halpert (1987) study was referenced in the revised manuscript on Page 4, Line 155 and linkage between ENSO and Indian rainfall through the Walker Circulation is now mentioned on Page 4, Line 155.

6. Figure 7, what monsoon rainfall is used, full monsoon or late monsoon?

The authors note that Figure 7 is the wavelet power spectrum of the All-India time series without any seasonal averaging.

7. Line 447, what is the abbreviation of AIR standing for?

The acronym stands for All-India Rainfall. The acronym is now presented when we discuss the All-India rainfall time series in the data section.

8. Line 135-137, keep the font format consistent.

The authors appreciate the identification of the formatting issue, which was corrected in the revised manuscript.

I recommend authors to do a search on [hydrology and wavelets and precipitation and "el Nino"] or maybe "low frequency variability" and see how they have established the link of their paper to the hydrology audience they are presenting to. It may give authors a good idea of how they could improve their pitch.

The authors appreciate the suggestion regarding a literature search. We conducted a literature search on wavelet analysis and hydrology and included the following references on Page 4 Line 142 because they focus on hydrological applications of wavelet coherence.

Carey, S. K., Tetzlaff, D., Buttle, J., Laudon, H., McDonnell, J,. McGuire, K., Seibert, J., Soulsby, C., Shanley, J. : Use of color maps and wavelet coherence to discern seasonal and inter annual climate influences on streamflow variability in northern catchments. Water Resources Research, 49, 6194–6207, 2013.

Holman, I. P., Rivas-Casado, M., Bloomfield, J.P., Gurdak, J. J.: Identifying nonstationary groundwater level response to North Atlantic ocean–atmosphere teleconnection patterns using wavelet coherence. Hydrogeol. J. http:// dx.doi.org/10.1007/s10040-011-0755-9, 2011.

Schaefli, B., Maraun, D., and Holschneider, M.: What drives high flow events in the Swiss Alps? Recent developments in wavelet spectral analysis and their application to hydrology, Adv. Water Resour., 30, 2511–2525, 2007.

Zhang, Q., Xu, C., Jiang, T., Wu, Y.: Possible influence of ENSO on annual maximum streamflow of the Yangtze River, China, Journal of Hydrol, 333, 265–274. doi:10.1016/ j.jhydrol.2006.08.010, 2007.

A Skewed perspective of the Indian rainfall-ENSO Relationship

Justin Schulte[1*], Fredrick Policielli[2], and Benjamin Zaitchik[3]

1. Science Systems and Applications, Inc.

2. NASA Goddard Space Flight Center

3. John Hopkins University

***corresponding Author: Justin Schulte (justin.a.schulte@nasa.gov)**

Abstract

~~The application of higher order wavelet analysis to India rainfall and the El Niño/Southern Oscillation (ENSO) is presented. An auto bicoherence analysis is used to extract the frequency modes contributing to the skewness of India rainfall and ENSO. A nonlinear wavelet coherence method is proposed for diagnosing why the time domain correlation between two time series temporally changes when at least one time series has changing nonlinear characteristics.~~

~~The results indicate the India rainfall and ENSO are highly nonlinear phenomenon. It is also demonstrated that the sea surface temperature (SST) patterns associated with different nonlinear ENSO modes depend on the frequency components participating in the nonlinear phase coupling. The SST pattern associated with coupling between ENSO modes with periods of 31 and 15.5 months is reminiscent of a central Pacific El Niño and intensifies around 1995, contrasting with the coupling between the 62- and 31- month modes that became active around the 1970s ENSO regime shift. A nonlinear coherence analysis showed that the skewness of India rainfall is weakly correlated with that of 4 ENSO time series after the 1970s, indicating that increases in ENSO skewness after 1970's at least partially contributed to the weakening India rainfall ENSO relationship in recent decades. The implication of this result is that the intensity of skewed El Niño events is likely to overestimate India drought severity, which was the case in the 1997 monsoon season, a time point when the nonlinear wavelet coherence between All India rainfall and ENSO reached its lowest value in the 1871-2016 period.~~

~~Wavelet coherence is a commonly used method in hydrology to extract scale dependent, non stationary relationships between time series. However, we show that the method cannot always determine why the time domain correlation between two time series temporally changes. We show that even for stationary coherence, the time domain correlation between two time series weakens if at least one of the time series has changing nonlinear characteristics. To overcome this drawback, a nonlinear coherence method is proposed for quantifying the cross correlation between nonlinear modes embedded in time series. It is shown that using nonlinear coherence spectra together with auto bicoherence spectra can provide additional insight into changing time domain correlations. The new method is applied to El Niño /Southern Oscillation (ENSO) and All India rainfall, which is closely linked to hydrological processes across the Indian sub continent. The nonlinear coherence analysis showed that the skewness of All India rainfall is weakly correlated with that of 4 ENSO time series after the 1970s, indicating that increases in ENSO skewness after the 1970s at least partially contributed to the weakening All-India rainfall-ENSO relationship in recent decades. The implication of this result is that the intensity of skewed El Niño events is likely to overestimate India drought severity, which was the case in the 1997 monsoon season, a time point when the nonlinear wavelet coherence between All India rainfall and ENSO reached its lowest value in the 1871-2016 period. We determined that the association between the weakening ENSO-All India rainfall relationship and ENSO nonlinearity could reflect the contribution of different nonlinear ENSO modes to ENSO diversity.~~

Wavelet coherence is a commonly used method in hydrology to extract scale-dependent, non-stationary relationships between time series. However, we show that the method cannot always determine why the time-domain correlation between two time series temporally changes. We show that even for stationary coherence, the time-domain correlation between two time series weakens if at least one of the time series has changing nonlinear characteristics. To overcome this drawback, a nonlinear coherence method is proposed for quantifying the cross-correlation between nonlinear

modes embedded in time series. It is shown that using nonlinear coherence spectra together with auto-bicoherence spectra can provide additional insight into changing time domain correlations. The new method is applied to El Niño /Southern Oscillation (ENSO) and All-India rainfall, which is closely linked to hydrological processes across the Indian sub-continent. The nonlinear coherence analysis showed that the skewness of All-India rainfall is weakly correlated with that of 4 ENSO time series after the 1970s, indicating that increases in ENSO skewness after the 1970s at least partially contributed to the weakening All-India rainfall-ENSO relationship in recent decades. The implication of this result is that the intensity of skewed El Niño events is likely to overestimate India drought severity, which was the case in the 1997 monsoon season, a time point when the nonlinear wavelet coherence between All-India rainfall and ENSO reached its lowest value in the 1871-2016 period. We determined that the association between the weakening ENSO-All India rainfall relationship and ENSO nonlinearity could reflect the contribution of different nonlinear ENSO modes to ENSO diversity.

1. Introduction

~~Precipitation variability across India is largely related to the seasonal Southwest and Northeast monsoon systems involving changes in the prevailing low level wind direction. Understanding the precipitation variability across India is complex because India rainfall is a non stationary, non linear phenomenon that is influenced by numerous large scale climate patterns such as the El Niño/Southern Oscillation (ENSO; Walker and Bliss, 1932) and the Indian Ocean Dipole (IOD; Ashok et al., 2001; Ashok et al., 2004) pattern. Predicting India rainfall has important implications for the agriculture, human health, and economy of India, making the Indian monsoon an active area of research despite early work on monsoon prediction extending back to the 1800s (Blanford, 1884).~~

~~An important source of predictability for the Indian monsoon is ENSO. During EL Niño years, droughts are favored, while rainfall surpluses are favored during La Niña years. However, there is no one to one relationship between ENSO and Indian rainfall. As a result, summer rainfall predictions based on ENSO have proven challenging. For example, the 1997/1998 EL Niño event was extremely strong yet climatological Indian monsoon conditions were observed (Shen and Kimoto, 1999; Slingo and Annamalai, 2000). It is therefore important to understand why certain El Niño events are not accompanied by monsoon failures.~~

South Asian Monsoon, the dominant source of precipitation for the Indian subcontinent, has been a target for seasonal prediction for well over a century (Blanford, 1884). Despite this long heritage of research, skillful prediction remains a challenge, driving extensive and ongoing research on statistically and dynamically-based prediction methods (e.g., REFS). It is difficult to overstate the importance of the South Asian Monsoon to well-being in India. Strong monsoon years are associated with catastrophic flooding (Kale, 2012; Sanyal and Lu, 2005) and large landslides (Dortch et al., 2009), while weak monsoons have led to water shortages (Mishra et al., 2016) and crop losses (Prasanna, 2014; Parthasarathy et al., 1988) that, in historical times, were known to result in significant food shortages (Fagan, 2009). Thus, while the majority of monsoon forecast studies target prediction of rainfall totals, the hydrological and agricultural impacts of monsoon variability provide the most pressing motivation for the work.

Much of the research on South Asian Monsoon prediction has focused on the relationship between the El Niño/Southern Oscillation (ENSO; Walker and Bliss, 1932) and monsoon strength. During El Niño years, droughts are favored, while rainfall surpluses are favored during La Niña years (Shukla and Paolino, 1983; Kripalani and Kulkarni, 1997). However, there is no one-to-one relationship between ENSO and Indian rainfall. As a result, summer rainfall predictions based on ENSO have proven challenging. For example, the 1997/1998 El Niño event was extremely strong yet climatological Indian monsoon conditions were observed (Shen and Kimoto, 1999; Slingo and Annamalai, 2000). It is therefore important to understand why certain El Niño events are not accompanied by monsoon failures.

There are a few reasons for the challenges faced when predicting Indian rainfall using ENSO. The first reason is that the relationship between ENSO and India rainfall is non-stationary. As shown by Torrence and Webster (1999), the relationship between ENSO and India rainfall cycles between periods of high and low coherence. Kumar et al. (1999) found that the relationship between India rainfall and ENSO weakened in the 1970s and hypothesized that a southward shift in Walker circulation anomalies associated with ENSO events and increased Eurasian spring and winter surface temperatures was responsible for the weakening relationship. Other work suggests that the changing

ENSO-India rainfall relationship was the result of tropical Atlantic sea surface temperatures (SSTs) and the Atlantic Multi-decadal Oscillation modulating the relationship (Lu et al., 2006; Kucharski et al. 2007; Kucharksi et al., 2009; Chen et al., 2010). In contrast, Kumar et al (2006) and Fan et al. (2017) argued that the occurrence of different ENSO flavors (Johnson, 2013) such as the Eastern Pacific and Central Pacific types could explain the changes in the ENSO-India rainfall relationship. Other investigators adopted another perspective to explain changes in the ENSO-India rainfall relationship and concluded that temporal undulations in the ENSO-India rainfall relationship are related to statistical under sampling and stochastic fluctuations (Gershunov et al. 2001; van Oldenborgh and Burgers, 2005; Delsole and Shukla, 2006; Cash et al., 2017). In a recent analysis, Yun and Timmermann (2018) showed that changes in the ENSO-Indian rainfall relationship are consistent with a stochastically perturbed ENSO signal and argued that changes in the ENSO-India monsoon relationship may not be related to external climate forcing mechanisms.

The second reason for the ENSO-related prediction challenges is that ENSO itself is a non-stationary phenomenon. Using wavelet analysis, Kestin et al. (1998) found that the interannual variability of ENSO from 1930 to 1960 was dominated by a 4- to 7- year periodicity, whereas for the time period from 1960 to 1990, the interannual variability was also dominated by a 2- to 5- year periodicity. A wavelet power spectral analysis conducted by Torrence and Webster (1999) and Schulte (2016a) showed that ENSO signal energy in the 2- to 7-year period band undulates, with the signal energy of the Niño 3.4 time series particularly pronounced after the 1960s (Schulte 2016a).

The nonlinear characteristics (e.g. skewness) of ENSO are also non-stationary and undergo interdecadal changes (Wu and Hsieh, 2003). Numerous studies have reported an ENSO regime shift in the 1970s in which ENSO began to evolve more nonlinearly than in previous decades (An, 2004; An and Jin 2004; An, 2009). It is a curious fact that the ENSO regime shift of the 1970s coincided with the weakening ENSO-India rainfall relationship as documented by Kumar et al. (1999). This observation begs the question as to whether nonlinear ENSO regime changes are related to changes in the ENSO-India rainfall relationship.

Various mechanisms have been proposed for explaining ENSO skewness. Kang and Kug (2002) suggested that the asymmetry between the magnitude of El Niño and La Niña events is related to the relative westward displacement of zonal wind stress anomalies during La Niña events compared to El Niño events. Jin et al., (2003) and An and Jin (2004) found that ENSO asymmetry is related to nonlinear dynamical heating (NDH), where the magnitude of NDH is related to the propagation characteristics of ENSO. During strong El Niño events like the 1982/1982 and 1997/1998 events, SST anomalies were found to propagate eastward, with the eastward propagation tending to produce more NDH compared to weak EL Niño events when NDH is minimal (An and Jin, 2004). Since the late 1970s there has been a propensity for eastward propagation characteristics of ENSO (Santoso et al., 2013), contrasting with the time period before the 1970s that consisted of the relatively weak El Niño events of 1957/1958 and 1972/1973 (An and Jin, 2004; An, 2009). More recently, Su et al. (2010) showed that vertical temperature advection may have an opposing effect on ENSO asymmetry and that the asymmetry in the extreme eastern equatorial Pacific is related to meridional ocean temperature advection.

Previous investigators have used different metrics to quantify ENSO asymmetry. To measure the nonlinear character of ENSO, An and Jin (2004) used time-domain metrics such as skewness and maximum potential intensity (MPI) to quantify the skewness of SST anomalies and the skewness of individual ENSO events, respectively. An (2004) applied a principal component analysis (PCA) to a 21- year moving window of tropical Pacific SST skewness and found that the first PCA mode is characterized by positive skewness across the eastern equatorial Pacific and negative skewness across the central equatorial Pacific. This pattern means that interdecadal changes in the nonlinearity of ENSO is associated with positively skewed SST anomalies across the eastern equatorial Pacific, implying that El Niño events are stronger than La Niña events. While the methods implemented in the aforementioned studies provided important insights, they cannot reveal the frequency modes of ENSO that are contributing to the skewness. Furthermore, the sliding-window approach is not local in the sense that it cannot quantify the strength of nonlinearity at a point in time because skewness is calculated using a set of observations over some time interval. While the MPI index does address the problem of quantifying the skewness of individual events, it also does not provide any information regarding the frequency components contributing to ENSO skewness.

Recognizing the limitations of time-domain approaches, Timmermann (2003) conducted a bi-spectral analysis of the Niño 3 anomaly time series, where a peak (f_1,f_2) in the bi-spectrum means there is statistical phase

dependence among oscillators with frequencies f_1, f_2, and $f_1 + f_2$. That bi-spectral analysis revealed statistically significant bi-spectral power at several frequency pairs, including (0.038, 0.038), (0.028, 0.028), (0.0225, 0.0225), (0.0045, 0.032), and (0.0045, 0.045) [month^{-1}]. The peaks (0.0045, 0.032), and (0.0045, 0.045) [months^{-1}] were identified with the nonlinear interactions among 18-year and 2-year variability. Although the analysis provided new insights, the Fourier-based analysis could not reveal how the nonlinear nature of ENSO changed with time, an important property to capture given how the nonlinear characteristics of ENSO are non-stationary (Santoso et al., 2013). Much like the cross-wavelet power (Maraun and Kurths, 2004) and time-domain covariance, bi-spectral power is not a bounded quantity and so high bi-spectral power does not always mean strong phase dependence.

In this study, the deficiencies associated with the above-mentioned techniques are addressed using higher-order wavelet analysis, which allows for the quantification of frequency-dependent and non-stationary nonlinearities in time series (Van Millagan, 2004, Elsayad, 2006; Schulte, 2016b). More specifically, the objectives of the paper are the following: 1) quantify the nonlinearity of ENSO and Indian rainfall using higher-order wavelet analysis together with recently developed statistical tests; (2) Determine if different nonlinear modes of ENSO are associated with distinct SST patterns; and (3) develop nonlinear wavelet coherence methods to test the hypothesis that the breakdown of the ENSO-India rainfall relationship in recent decades is related to the shift of ENSO from a linear regime to a nonlinear one. The paper is organized as follows: In Section 2, data used are described. Section 3 includes the description of the implemented methodologies. Results are presented in Section 4 and concluding remarks are provided in Section 5.

2. Data

~~Monthly rainfall data for 5 homogenous regions (Parthasarathy et al. 1995a) were obtained from the Indian Institute of Tropical Meteorology website (http://www.tropmet.res.in). The five homogenous regions called the Peninsula, Northwest, Northeast, Central Northeast and West Central regions were constructed based on attributes such as contribution to annual rainfall amount and regional/global circulation parameters (Parthasarathy et al. 1995a; Azad et al., 2010). The variability of India rainfall was also analyzed using the all-India (Parthasarathy et al. 1995b) rainfall time series, which is created by averaging representative rain gauges at various locations across India (Mooley and Parthasarathy, 1984). The full monsoon season (June-September) and the late monsoon (August-September) season were used to identify possible within-season variations in the relationships. All 6 rainfall time series considered are continuous and span the time period from 1871 to 2016. To remove the influence of the annual cycle, the time series was converted into anomaly time series by subtracting the 1871-2016 long-term mean for each month from the individual monthly values. The anomaly time series were subsequently standardized by dividing them by their respective 1871-2016 standard deviations. Because wavelet analysis focuses on specific frequency components that are not impacted by long-term time-domain trends, no detrending of the data was performed.~~

The variability of India rainfall from 1871-2016 was analyzed using the All-India (Parthasarathy et al. 1994) rainfall time series, which was created by averaging representative rain gauges at various locations across India. The full monsoon season (June-September) and the late monsoon (August-September) season were used to identify possible within-season variations in the ENSO-All-India relationships. To remove the influence of the annual cycle, the time series was converted into anomaly time series by subtracting the 1871-2016 long-term mean for each month from the individual monthly values. The anomaly time series were subsequently standardized by dividing it by its 1871-2016 standard deviations. Because wavelet analysis focuses on specific frequency components that are not impacted by long-term time-domain trends, no detrending of the data was performed.

The monthly data for the Niño 1+2, Niño 3, Niño 3.4, and Niño 4 indices (available at: https://www.esrl.noaa.gov/psd/gcos_wgsp/Timeseries/Data/nino34.long.data) from 1871 to 2016 were used to understand how the nonlinear characteristics of SSTs vary from one ENSO region to another. The Niño 1+2 index is the average SST in the region with latitudinal boundaries 0° and 10°S and longitudinal boundaries 90°W and 80°W and the Niño 3 index is the average SSTs in the region with latitudinal boundaries 5°N and 5°S and longitudinal boundaries 150°W and 90°W. Variations in SSTs further west were described using the Niño 3.4 and Niño 4 indices, where the Niño 3.4 index is defined as the average SST in the region bounded by 5°N and 5°S and 170°W and 120°W and the Niño 4 index is defined as average SSTs in the region bounded by 5°N and 5°S and 160°E and 150°W. The

seasonal cycle was removed from these time series in the same way as it was removed from the rainfall time series. Like the rainfall data, these data were not detrended.

The monthly SST data from 1871-2016 were based on the Hadley Centre Global Sea Ice and Sea Surface Temperature (HadISST1; Rayner et al., 2003) The data at each grid point were converted to monthly anomalies in the same way as they were computed for the ENSO and All-India time series.

3. Methods

~~3.1 Event Decomposition~~

~~To quantify the time-domain skewness of individual ENSO and India rainfall events, the ENSO and rainfall time series were first decomposed into individual events using the event decomposition procedure outlined by Schulte and Lee (2019). That is, a time series $x_1,x_2,\ldots,x_N$ with data points located at the time points $t_1, t_2,\ldots,t_N$ was partitioned into subsequences comprising adjacent data points whose values are negative in the case of negative events and whose values are positive in the case of positive events. A positive event was considered to begin at t_i if $x_i > 0$ and $x_{i-1} < 0$. The decay phase of a positive event beginning at x_i was then defined as the time point t_j such that $t_j \geq t_i$, $x_j > 0$, $x_{j+1} < 0$, and $x_k > 0$ for all k such that $i \leq k \leq j$. Negative events were identified by switching the inequalities in the statements above. After the event decompositions, the peak intensity of events was calculated, where the peak intensity of a negative (positive) event was the minimum (maximum) value obtained by a data point within the event period $[t_i, t_j]$. The persistence of an event was defined as the number of points composing the event and the event intensity was defined as~~

~~$$I = \sum_{i=1}^{M} y_i \quad (1)$$~~

~~where the y_i are the M data points composing the event. The duration and intensity of events were depicted using event spectra (Schulte and Lee, 2019).~~

3.2 Wavelet Analysis

To better diagnose changes in time series statistics associated with India rainfall and ENSO, we adopted a wavelet analysis. ~~For a time series, X, comprising data points $x_1, x_2, \ldots, x_N$, the continuous wavelet transform is given by~~

~~The continuous wavelet transform of a time series $X = \{x_n : n = 1,2,..N\}$ is given by~~

$$W_n(s) = \sqrt{\frac{\delta t}{s}} \sum_{n'=1}^{N} x_{n'}\, \psi_0 \left[(n' - n)\frac{\delta t}{s}\right] \quad (2)$$

where s is wavelet scale, ψ_0 is an analyzing wavelet, δt is a time step (1 month in this study), and n is time. The sample wavelet power spectrum $|W_n(s)|^2$ measures the energy content of a signal at time n and scale s. The commonly used Morlet wavelet with angular frequency ω = 6 was used throughout this paper because it balances time and frequency localization ~~and because it is commonly used in hydrological and climate studies (Schaefli et al., 2007; Zhang et al., 2007;Holman et al., 2001; Carey et al., 2013)~~. The reader is referred to Torrence and Compo (1998) and Grinsted et al. (2004) for details about wavelet analysis.

Wavelet coherence was used to quantify the linear relationship between two time series as a function of frequency and time. Wavelet coherence between two time series X and Y is given by

$$R_n^2(s) = \frac{\left|S s^{-1} W_n^{XY}(s)\right|^2}{S\left(s^{-1}\left|W_n^X(s)\right|^2\right) S\left(s^{-1}\left|W_n^Y(s)\right|^2\right)}, \quad (3)$$

where S is a smoothing operator (Grinsted et al., 2004) and $W_n^{XY}(s)$ is the cross-wavelet power spectrum. ~~A coherence value of 1 indicates the strongest possible association between two variables at the scale s and time n. Large values of wavelet coherence correspond to time points and scales for which the relative phase difference between two time series varies little over a time interval. That is, two time series are perfectly coherent at the scale s if for some constant~~

~~c $\phi_n^X(s) - \phi_n^Y(s) = c$, where $\phi_n^X(s)$ is the phase associated with X and $\phi_n^Y(s)$ is the phase associated with Y. If the relative phase relationship is sufficiently stable, then the wavelet coherence will emerge as statistically significant (Section 3.4).~~ Two time series are perfectly coherent ($R_n^2(s) = 1$) at s if $\phi_n^X(s) - \phi_n^Y(s) = c$ over a sufficiently long time interval, where c is a constant, $\phi_n^X(s)$ is the phase associated with X, and $\phi_n^Y(s)$ is the phase associated with Y.

In the context of the Indian monsoon, strong coherence between rainfall and a climate pattern (e.g. ENSO) at a scale s indicates shared temporal characteristics between a climate pattern and rainfall. Because theory supports a causal link between ENSO and monsoon variability through changes in the Walker Circulation (Ropelewski and Halpert, 1987), strong coherence means that ENSO modulates rainfall. That is, when ENSO is in a warm phase at the scale s, negative rainfall anomalies are preferred; when ENSO is in a cool phase, the preference is reversed. As a result, the rainfall time series will inherit the temporal characteristics of the climate forcing time series at a scale s. If the climate forcing time series is strongly periodic, then the otherwise noisy rainfall time series could become periodic as well.

3.3 Higher-order Wavelet Analysis

Although the wavelet power spectrum is useful for quantifying the signal energy at a scale s and time n, it cannot determine if there is a nonlinear relationship among different frequency components. In fact, the power spectrum can only fully describe time series in frequency space in the case of linear systems in which the output is proportional to the input (King, 1998). For nonlinear systems, higher-order moments exist, and the frequency decomposition of higher-order moments such as skewness is necessary for a more complete description of the time series. Thus, higher-order wavelet methods were adopted to determine the frequency components contributing skewness without assuming stationarity like Fourier-based bicoherence analysis.

~~The type of nonlinearities that produce skewness are quadratic nonlinearities.~~ The type of nonlinearities considered in this study were quadratic nonlinearities in which the scales s_1, s_2, and s_3 satisfy the sum rule

$$\frac{1}{s_3} = \frac{1}{s_1} + \frac{1}{s_2} \tag{4}$$

and the wavelet phases satisfy

$$\phi_n(s_3) = \phi_n(s_1) + \phi_n(s_2). \tag{5}$$

These types of nonlinearities arise, for example, when a sinusoid is squared, in which case a harmonic is produced.

In this paper, quadratic nonlinearities giving rise to time series skewness were quantified using local and global wavelet-based auto-bicoherence methods (Schulte, 2016b). ~~In this paper, the frequency components contributing to the skewness and quadratic nonlinearities giving rise to time series skewness of a times series were quantified using local and global wavelet-based auto-bicoherence methods (Schulte, 2016b).~~ Global auto-bicoherence was computed using the equation

$$bi_{global}^X(s_1, s_2) = \frac{\left|B_{global}^X(s_1 s_2)\right|^2}{\left(\sum_{n=1}^N |W_n^X(s_1) W_n^X(s_2)|^2\right)\left(\sum_{n=1}^N |W_n^X(s_3)|^2\right)}, \tag{6}$$

where

$$B_{global}^X(s_1, s_2) = \sum_{n=1}^N \widehat{W}_n^X(s_3) W_n^X(s_1) W_n^X(s_2) \tag{7}$$

is the global bi-spectrum and the hat denotes the complex conjugate. Identical to wavelet coherence, auto-bicoherence is bounded by 0 and 1, a value of 1 indicating the strongest possible phase coupling among the phases $\phi_n(s_3)$, $\phi_n(s_2)$, and $\phi_n(s_1)$ such that sum rule Eq. (5) is satisfied. A peak in the auto-coherence spectrum at (s_1, s_2) means there is phase coupling between oscillatory modes with scales s_1, s_2, and s_3. High auto-bicoherence at (s_1, s_2) can also mean that the same oscillatory modes are contributing to the skewness of the time series. It is important to note that the auto-bicoherence cannot detect other types of nonlinearities such as cubic nonlinearities whose detection would require trisepctra (Collis et al., 1998).

~~While the global auto-bicoherence spectrum is useful for identifying nonlinear triads, it cannot determine how the strength of phase coupling changes with time.~~ To determine if the strength of the quadratic phase coupling change~~d~~s temporally, the local auto-bicoherence spectrum (Schulte, 2016b) given by

$$bi_n^X(s_1, s_1) = \frac{|Ss_1^{-1} B_{local}(s_1, s_1)|^2}{S\left(s_1^{-1}|W_n^X(s_1) W_n^X(s_1)|^2\right) S\left(s_1^{-1}\left|W_n^X\left(\frac{s_1}{2}\right)\right|^2\right)} \quad (8)$$

was computed, where $B_n^X(s_1, s_2)$ is the local bi-spectrum given as

$$B_n^X(s_1, s_{12}) = \widehat{W}_n^X(s_3) W_n^X(s_1) W_n^X(s_1). \quad (9)$$

~~In this study, we focused on the local diagonal slices of the auto-bicoherence spectrum, which consists of all points such that $s_1 = s_2$ so that Eq. (4) implies that~~ and $s_3 = s_1/2$. In this special case, the local auto-bicoherence spectrum ~~was calculated using the equation~~

~~$$bi_n^X(s_1, s_1) = \frac{|Ss_1^{-1} B_{local}(s_1, s_1)|^2}{S\left(s_1^{-1}|W_n^X(s_1) W_n^X(s_1)|^2\right) S\left(s_1^{-1}\left|W_n^X\left(\frac{s_1}{2}\right)\right|^2\right)} \quad (10)$$~~

~~to~~ reveal~~ed~~ the time-evolution of auto-bicoherence estimates located along the diagonal slice in the global spectra. Local Bi-phase ~~corresponding to each point in the local auto-bicoherence spectrum was used to quantify the local cycle geometry of the time series. Local bi-phase is given by~~

$$\psi_n(s_1, s_2) = \phi_n(s_1) + \phi_n(s_2) - \phi_n(s_3) \quad (11)$$

~~and~~ was used to measure~~s~~ the skewness and asymmetries of waveforms. A bi-phase of 0◦ means that the relationship among the scale components produces positive skewness with respect to a horizonal axis so that positive deviations from the mean are larger than negative deviations from the mean. On the other hand, a bi-phase of 180◦ indicates negative skewness with respect to the mean. Bi-phases near -90◦ or 90◦ indicate the presence of asymmetric cycle geometry (King, 1998; Maccarone, 2014; Schulte, 2016b), indicating that a time series rises (falls) more quickly than it falls (arises).

To be consistent with the wavelet power and coherence analyses, results for the higher-order wavelet analysis were casted in terms of Fourier period rather than wavelet scale. The Fourier period corresponding to s_i was denoted by p_i, where the Fourier period is obtained by multiplying s_i by 1.03 for the Morlet wavelet (Torrence and Compo, 1998). Thus, the local diagonal slice of the auto-bicoherence spectra were plotted using the Fourier period p_1 corresponding to s_1 as the vertical axis and time as the horizonal axis. High (or statistically significant) local auto-bicoherence at p_1 and time n means that there is phase dependence between modes with periods p_1 and $p_1/2$ at time n because $2p_3 = p_1$ according to Eq. (4) when $p_1 = p_2$. In other words, the local diagonal slice determines if there is phase coupling between an oscillatory mode and its harmonic at various time points.

3.4 Statistical Hypothesis Testing

The statistical significance of all wavelet spectra was evaluated using the cumulative area-wise test (Schulte, 2016a; Schulte, 2018) to account for the simultaneous testing of multiple hypotheses (Maraun and Kurths, 2004; Maraun et al., 2014). This test evaluated the statistical significance of points in the wavelet domain based on the area of contiguous regions of point-wise significance to which they belong so that larger area implies greater statistical significance. Given that patch area can changes as the point-wise significance changes, the cumulative area-wise test evaluates signifcacne based on the area of patch averaged across a set of point-wise significance levels (Schulte, 2019) ~~To perform the cumulative area-wise test, the point-wise test p-values associated with all points in the wavelet domain had to be estimated using theoretical red-noise backgrounds for wavelet power and Monte Carlo methods for wavelet coherence and auto-bicoherence (Torrence and Compo, 1998, Grinsted et al., 2004, Schulte 2016b). After the point-wise test implementations, the cumulative area-wise test was used to assess the statistical significance of points in the wavelet domain by tracking how the normalized area of contiguous regions of point-wise significance changed as the point-wise significance level was varied.~~ The test was applied at the 5% cumulative area-wise significance level using point-wise significance levels ranging from 0.02 to 0.1~~9~~8 because this choice of point-wise significance levels

was shown to result in the cumulative area-wise test outperforming the point-wise test in terms of true positive detection for high signal-to-noise ratios despite how the cumulative area-wise test is more stringent. The test was performed using the Advanced Biwavelet Wavelet R software Package (available at: http://justinschulte.com/wavelets/advbiwavelet.html).Technical details of the testing procedure can be found in Schulte (20198) and in Appendix A.

To assess the statistical significance of the global auto-bicoherence estimates, a modified version of the cumulative area-wise test was applied. In the modified version of the cumulative area-wise test, the normalized area of patches was computed by dividing patch area by the product $\widehat{s_1}\widehat{s_2}$, where $\widehat{s_1}$ is the mean first-coordinate of the patch and $\widehat{s_2}$ is the mean second coordinate. The means were calculated by assuming that the point-wise significance regions are polygons with a set of vertices (Schulte et al., 2015). The reason for this modified normalized area is that dividing area by say, $\widehat{s_1}^2$, retained the correlation between normalized area and s_2. The test was applied using the same point-wise significance levels that were used to assess the statistical significance of wavelet power and coherence.

~~To further assess statistical significance of wavelet quantities, a topological significance test (Schulte et al. 2015; Schulte 2018) and a cumulative arc wise test was also applied to the wavelet spectra. The implementation of the topological significance test involved the computation of the number of holes and contiguous point wise significance regions at a discrete set of point wise significance levels, resulting in persistent homology profiles. The topological significance and cumulative arc wise tests were applied at the 5% significance level, and the point wise significance levels used ranged from 0.02 to 0.98. The critical levels of the test were estimated using Monte Carlo methods by generating 1000 realizations of a red noise process with lag 1 auto correlation coefficients equal to that of the input time series.~~

3.5 Higher-order Coherence

Although wavelet coherence spectra can provide information regarding how the relationship between two climate variables changes at a scale *s*, it cannot completely explain why the time-domain correlation between the climate variables temporally fluctuates. The reason is that linear wavelet coherence only examines how well the variance of one time series corresponds to the variance of another at a scale *s* because linear coherence is determined by the wavelet power spectra of the time series. That is, linear coherence between two climate variables means that larger fluctuations in one time series produce larger fluctuations of another climate variable at the scale *s*. However, for two time series to be perfectly correlated in the time domain, higher skewness of one climate variable must also correspond to higher skewness of the other climate variable.

Recognizing that skewness is important for better understanding time-domain correlation changes, the quantity

$$Bi_n^2(s) = \frac{\left|Ss_{smooth}^{-1} B_n^{XY}(s_1,s_2)\right|^2}{S\left(s_{smooth}^{-1}\left|B_n^X(s_1,s_2)\right|^2\right) S\left(s_{smooth}^{-1}\left|B_n^Y(s_1,s_2)\right|^2\right)}, \quad (12)$$

called third-order coherence (nonlinear coherence, hereafter) was used to determine if changes in the skewness of X are associated with changes in the skewness of Y (see Appendix B for a more general definition). In Eq, (12), s_{mooth} is one of the three scales, and $B_n^{XY}(s_1, s_2)$ is the third-order cross-wavelet power spectrum, which is the product of the bi-spectrum of X and the conjugate of the bi-spectrum of Y, the higher-order analog of the cross-wavelet power spectrum. The word cross-bispectrum was not used to avoid confusion with cross-bicoherence analysis (Van Milligen,1995). Like wavelet coherence, the nonlinear coherence is bounded by 0 and 1, a value of 1 indicating that the bi-spectra of X and Y at (s_1, s_2) are perfectly and linearly correlated. The statistical significance of nonlinear coherence was assessed using Monte Carlo methods and the cumulative area-wise test in the same way as it was used to assess the statistical significance of wavelet coherence.

Another way to interpret higher-order wavelet coherence is using linear and nonlinear modes. A linear mode $\gamma_{s_i}^X$ is the signal component of X at the scale s_i obtained by setting all wavelet coefficients to zero except those at s_i and taking the inverse wavelet transform of the result. Because linear modes are only composed of a single frequency component, the local cross-correlation (coherence) between $\gamma_{s_i}^X$ and $\gamma_{s_i}^Y$ is only impacted by the variances of X and Y

at s_i. On the other hand, nonlinear coherence measures the local cross-correlation between the skewness of $\gamma_{s_1}^X + \gamma_{s_2}^X + \gamma_{s_3}^X$ and $\gamma_{s_1}^Y + \gamma_{s_2}^Y + \gamma_{s_3}^Y$ or between $\gamma_{s_1}^X + \gamma_{s_{1/2}}^X$ and $\gamma_{s_1}^Y + \gamma_{s_{1/2}}^Y$ in the case that $s_1 = s_2$.

To better understand nonlinear coherence, we supposed that

$$\phi_n^X(s_1) - \phi_n^Y(s_1) = c_1 \tag{13}$$

$$\phi_n^X(s_2) - \phi_n^Y(s_2) = c_2 \tag{14}$$

$$\phi_n^X(s_3) - \phi_n^Y(s_3) = c_3 \tag{15}$$

for constants c_1, c_2, and c_3. Adding Eqs. (13) and (14) and subtracting Eq. (15) from the result produced the equality

$$\phi_n^X(s_1) + \phi_n^X(s_2) - \phi_n^X(s_3) - (\phi_n^Y(s_1) + \phi_n^Y(s_2) - \phi_n^Y(s_3)) =$$

$$\psi_n^X(s_1, s_2) - \psi_n^Y(s_1, s_2) = \psi_n^{bi}(s_1, s_2) = K\,, \tag{16}$$

for some constant $K = c_1 + c_2 - c_3$. Thus, if *X* is perfectly nonlinear coherent with *Y*, then *X* and *Y* must be perfectly coherent at the three scales participating in the phase coupling. Even if the coherence is perfect at two scales, the relative bi-phase $\psi_n^{bi}(s_1, s_2)$ will fluctuate randomly if the relative phase difference at the remaining scale fluctuates randomly so that the nonlinear coherence will be low. Thus, if nonlinear coherence is high, then there must be some non-random relationship between *X* and *Y* at all three scales even if high linear coherence was not identified at one or more scales. This theoretical idea suggests that nonlinear coherence can uncover relationships that linear coherence cannot (see Figure S1 in supplementary material).

The relative bi-phase difference $\psi_n^{bi}(s_1, s_2)$ is the higher-order analog of the relative phase difference between two time series. It measures how much the cycle geometry of one time series lags that of another. A lagged bi-phase of 180◦ means that the skewness or asymmetry of the forcing time series is opposite to that of the response. For example, if the forcing has positive skewness, then the response will have negative skewness. If the relative bi-phase is 0◦, then negative (positive) skewness of the forcing produces negative (positive) skewness of the response, contributing to the positive time-domain correlation between the time series. Scales and time points for which nonlinear coherence is high are where the relative bi-phase is stable.

Throughout this paper, we will focus on nonlinear coherence computed along the diagonal slices ($p_1 = p_2$) of the time series bi-spectra. The nonlinear coherence spectra are then plotted using p_1 as the vertical axis and time as the horizonal axis. High nonlinear coherence at p_1 and *n* means that the skewness or asymmetry between $\gamma_{p_1}^X + \gamma_{p_{1/2}}^X$ and $\gamma_{p_1}^Y + \gamma_{p_{1/2}}^Y$ are locally cross-correlated.

To demonstrate the concept of nonlinear coherence, we considered a simple example in which the nonlinear climate forcing time series was given by

$$F(t) = \cos(\frac{2\pi}{p_1} t + \varphi) + \gamma\,(t) \cos(\frac{2\pi}{p_3} \mathrm{t} + 2\varphi) + W_F(t) \tag{17}$$

and the response to the forcing was given as

$$R(t) = \cos(\frac{2\pi}{p_1} t + \varphi) + w_R(t), \tag{18}$$

In Eq. (17), $\gamma\,(t)$ is a time-varying nonlinear coefficient, $w_F(t)$ is Gaussian white noise associated with the forcing, $w_R(t)$ is Gaussian white noise associated with the response, $\varphi = 0$ is phase, and $p_1 = 2p_3 = 32$. The nonlinear coefficient was assumed to be a linear function of time, i.e.,

$$\gamma(t) = t/500. \tag{19}$$

The effect of the coefficient is to linearly increase the variance of $F(t)$ at $p_3 = 16$ and increase the strength of the quadratic phase coupling between the modes with periods $p_3 = p_1/2 = 16$ and $p_1 = 32$.

As shown in Figure 1a, $F(t)$ (black curve) and $R(t)$ (thick green curve) evolve coherently from t = 0 to t = 200. After t = 200, $F(t)$ begins to noticeably exceed $R(t)$ at certain time points (e.g. t = 430) while the relationship between them at other points is reversed (e.g. t = 450) in the sense that a positive forcing produces a negative response. As a result, the correlation between $F(t)$ and $R(t)$ weakens (Figure 1b). An inspection of the wavelet coherence spectrum (Figure 2a) reveals that the coherence at p_1 = 32 is strong and stable so that changes in the relationship strength at that time scale is not the cause of the weakening time-domain correlation. The coherence at all other periods is also stationary by construction so that it is not the changing relationship strength at any scale that is causing the time-domain correlation weakening. However, the variance of $F(t)$ at p_3 = 16 increases with time (not shown) and the coherence between $F(t)$ and $R(t)$ is also weak at that time scale, implying that larger fluctuations in $F(t)$ at p_3 = 16 are not accompanied by larger fluctuations in $R(t)$. Thus, variance increase of $F(t)$ is one reason for the weakening time-domain correlation. However, both linear coherence and wavelet power cannot explain why the skewness of $F(t)$ increases, while the skewness of $R(t)$ is relatively stable (Figure 1c).

To further diagnose a cause of the weakening time-domain correlation, it is necessary to look at the auto-bicoherence spectrum of $F(t)$ and the nonlinear wavelet coherence spectrum. An inspection of the local auto-bicoherence spectrum of $F(t)$ (Figure 2b) reveals that the auto-bicoherence at p_1 = 32 is increasing with time, indicating that the phase coupling between modes with periods p_3 = 16 and p_1= 32 is strengthening with time. The bi-phase of 0◦, as indicated by arrows pointing to the right, confirms that the phase coupling is contributing to the positive skewness seen in Figure 1a to an increasing degree. Furthermore, the nonlinear coherence between $R(t)$ and $F(t)$ is weak and mostly statistically insignificant at p_3= 32 (Figure 2c), implying that the skewness of $F(t)$ produced from the phase coupling between the modes p_3 = 16 and p_1 = 32 does not influence the skewness of $R(t)$. In other words, the skewness of $\gamma_{16}^F + \gamma_{32}^F$ is uncorrelated with the skewness of $\gamma_{16}^R + \gamma_{32}^R$, where $\gamma_{16}^F + \gamma_{32}^F$ is the sum of the cosines in Eq. (17) and the components of $W_F(t)$ at p_3 = 16 and p_1 = 32. The nonlinear mode $\gamma_{16}^R + \gamma_{32}^R$ is the sum of the cosine in Eq. (18) and the components of $w_R(t)$ at p_3 = 16 and p_1= 32. The weak nonlinear coherence also means that $\psi_n^F(32,32) - \psi_n^R(32,32)$ fluctuates randomly (not shown). Thus, the skewness of $R(t)$ in the time-domain is practically uncorrelated with the skewness of $F(t)$ because the skewness of $F(t)$ is solely related to the phase coupling between the modes with periods p_3 = 16 and p_1 = 32 Thus, the increase in skewness of $F(t)$ also contributes to the weakening time-domain correlation.

The lack of nonlinear coherence at time scales for which $F(t)$ is nonlinear has implications for empirical prediction. At time points when $F(t)$ is positively skewed $R(t)$ is overestimated because $R(t)$ is not inheriting the skewness of $F(t)$. In other words, a large forcing produces an unexpectedly small response. That is, if one created a linear regression model based on the relationship between $F(t)$ and $R(t)$ from t = 0 to t =200 one would find that a forcing value of, say, 1 would produce a response close to 1. If the same model was used to predict $R(t)$ at, say, t = 430 one would predict that the forcing with value around 2 should result in a response near 2. However, because the relatively large value $F(430)$ results from skewness and $R(t)$ is uncorrelated with its skewness, the response is only as strong as the part of $F(t)$ not resulting from the quadratic phase coupling. The more nonlinear $F(t)$ becomes, the more $F(t)$ will overestimate $R(t)$ when $F(t)$ is positively skewed. Similarly, the positive forcing produces a negative response at t = 450 because of skewness and not simply a change in variance. Nonlinear coherence allows for the quantification and identification of these time-domain aberrations.

The weakening relationship shown in Figure 1b could lead a researcher studying a hydrological process to believe that another direct forcing mechanism must be directly influencing the hydrological process. This belief could lead to the applications of partial coherence (Ng, and Chan, 2012) and partial correlation analyses to identify another influential forcing mechanism. However, in this case, there are no other direct forcing mechanisms; the weakening time-domain relationship is solely related to how $F(t)$ transitioned from a linear regime ~~process~~ to a nonlinear regime. This theoretical result suggests that hydrological studies using wavelet coherence should also consider the nonlinearity of the times series. ~~process. That is, the change is related entirely to how the skewness of $F(t)$ changed. However, the phenomena influencing the linearity of $F(t)$ would be at least indirectly related to $R(t)$~~).

4. Results

4.1 ~~Event Decomposition of~~ ENSO and Indian Monsoon time series

The time series of the Niño 1+2 and Niño 4 indices ~~together with the corresponding event spectra~~ are shown in Figures 3 ~~and Figures 4~~, where we have chosen to show the results for the Niño 4 and Niño 1+2 indices because they provide contrasting results. For the Niño 1+2 time series, a few recent notably intense (Figure 3b) warm events are located around 1982/1983, 1997/1998, and 2015/2016 coinciding with the strongest El Niño events in recent decades (McPhaden, 1999, Hu and Fedorov, 2017; Santoso et al, 2017). ~~The event spectra for the Niño 3 and Niño 3.4 indices identified notably intense warm events that occurred after the 1970s (not shown).~~ A few notably intense events were also found in the late 1800s and early 1900s, indicating that intense ENSO events are not unique to recent decades. ~~Also evident from an inspection of Figure 3a is that the recent intense Niño 1+2 events are also skewed in the sense that they are stronger than the surrounding cool Niño 1+2 events. Thus, it appears that the skewness of the Niño 1+2 time series has increased in recent decades.~~

~~To visualize how skewness changes temporally,~~ The ~~a~~ 20-year sliding skewness ~~analysis was conducted. As shown in Figure 5a, the skewness of~~ time series the Niño 1+2 index reveals ~~is~~ enhanced skewness during the early 1880s, near zero skewness around the 1930's and early 1940's, and especially enhanced skewness after the 1970s. It also appears that there is an upward trend in skewness beginning around the 1940s, where the skewness peaks around 2000. In contrast to the Niño 1+2 index, the skewness of the Niño 4 index becomes more negative after the 1970s, and the magnitude of the skewness is generally smaller than that of the Niño 1+2 time series. This finding suggests that the transition of the Niño 1+2 time series to a nonlinear regime was more pronounced than the transition associated with the Niño 4 time series. Interestingly, a 20-year sliding skewness analysis of All-India rainfall reveals that the skewness of June-September All-India rainfall ~~remains close to zero until the 1990s despite the upward trend in Niño 1+2 skewness beginning in the 1940s (Figure 5a).~~ ~~Similarly, the skewness of August-September All-rainfall anomalies does not increase to the extent that Nino 1+2 skewness does, though the skewness does seem to be negatively correlated with the skewness of the Nino 4 index after the 1970s, consistent with how the All-Raifnall rainfall and the Nino 4 are negatively correlated.~~ ~~However, T~~the skewness of June-September All-India rainfall becomes more negative in the 1990s and 2000s, but it is unclear if that negative skewness is related to ENSO, noise, or another climate pattern ~~because the skewness of the Niño 1+2 and Niño 4 indices do not change as abruptly. Negative June-September All-India rainfall skewness is accompanied by enhanced positive skewness of the Niño 1+2 indices prior to the 1940s, which is consistent with how All-India rainfall is negatively correlated with the Niño 1+2 index time series during that time period (Figures 5b and 5c). Our results suggest that All-India rainfall skewness is more correlated with ENSO skewness prior to the 1930s than it is in recent decades.

4.2 The time-domain Indian Rainfall-ENSO Relationship.

~~Given the non stationaries in skewness can influence the time domain correlation between two time series (Figure 1b), it is reasonable to hypothesize that the All India rainfall relationship with the Niño 1+2 and Niño 4 indices could be non stationary given that changes in Indian rainfall skewness do not always correspond with changes in ENSO skewness. To test the hypothesis, a 20 year sliding correlation analysis was conducted between these ENSO indices and All India rainfall for the full (June September) and late monsoon (August September) seasons. The correlation between the time series of the Niño 1+2 and Niño 4 indices and All India rainfall was computed directly without seasonal averaging.~~

~~As shown in Figure 5b, the relationship between full season India rainfall and the Niño 1+2 index generally weakens from the 1800's to the 2000s. In contrast, the Niño 4 index relationship with All India rainfall for the full season appears to have no long term trend, resulting in the Niño 4 index becoming more strongly correlated with All India rainfall than the Niño 1+2 index after the 1970's. The relationship between Indian rainfall and time series for the Niño 3 and Niño 3.4 indices was also found to be relatively weak after the 1970s (not shown).~~

~~The stronger relationship between All India rainfall and the Niño 4 index compared to the Niño 1+2 relationship with All India rainfall after the 1970s is more evident in the late season analysis (Figure 5c). An abrupt weakening of the Niño 1+2 rainfall relationship occurs around the 1970's, with the relationship reversing around the 1990s. A comparison of Figures 5a and Figures 5c reveals that the weakening and reversal of the relationship occurs during the time period when the Niño 1+2 index is especially skewed, suggesting that ENSO skewness changes could be contributing to changes in the time domain correlation between ENSO and All India rainfall. However, we have not shown that ENSO skewness exceeds a red noise background (Sections 4.2 and 4.3) so that ENSO skewness~~

changes and time domain correlation impacts could still be noise and unpredictable. Nevertheless, this reversal is consistent with how Fan et al. (2017) found that the SST composite difference between drought and drought-free El Niño years during the 1979-2012 period features warming across the central equatorial Pacific and cooling across the eastern equatorial Pacific, whereas the SST composite for the 1978-1987 period features warming across the eastern to central equatorial Pacific. It also noted that Niño 1+2 index-rainfall relationship is also relatively weak during the late 1800's when Niño 1+2 skewness is relatively high (Figure 5a).

A rapid weakening is also seen in the Niño 4-rainfall relationship, but it appears to begin in the 1980's, which is later than the Niño 1+2 rainfall relationship breakdown. Nevertheless, the weakening Niño 4-India rainfall relationship coincides with the enhanced negative skewness of the Niño 4 index (Figures 5a). The fact that Niño 1+2 skewness is greater than Niño 4 skewness after 1970s and that the Niño 1+2 index relationship with All-India rainfall weakens more abruptly than the Niño 4 index relationship with All-India rainfall suggests that skewness could at least partially explain the temporal fluctuations in the relationships seen in Figure 5. Thus, a further investigation is needed to better understand the temporal changes in ENSO statistics and their impact on the ENSO-India rainfall relationship.

The differences in skewness shown in Figure 4 suggests that the correlation between the ENSO time series and All-India rainfall breaks down after the 1970s, which is confirmed by the 20-year sliding correlation between June-September All-India India rainfall and ENSO indices (Figure 5). The relationship with the Niño 1+2 generally weakens from the 1800's to the 2000s. In contrast, the June-September Niño 4 index relationship with All-India rainfall appears to have no long-term trend, resulting in the Niño 4 index becoming more strongly correlated with All-India rainfall than the Niño 1+2 index after the 1970's. The relationship between All-India rainfall and time series for the Niño 3 and Niño 3.4 indices was also found to be relatively weak after the 1970s (not shown).

The stronger relationship between All-India rainfall and the Niño 4 index compared to the Niño 1+2 index relationship with All-India rainfall after the 1970s is more evident in the August-September analysis (Figure 5b). An abrupt weakening of the Niño 1+2-All-India rainfall relationship occurs around the 1970's, with the relationship reversing around the 1990s. A comparison of Figures 4b and Figures 5b reveals that the weakening and reversal of the relationship occurs during the time period when the Niño 1+2 index is especially skewed. The fact that the Niño 1+2 skewness is greater than Niño 4 skewness after 1970s and that the August-September Niño 1+2 index relationship with August-September All-India rainfall weakens more abruptly than the August-September Niño 4 index relationship with August-September All-India rainfall suggests that changes in ENSO skewness could at least partially explain the temporal fluctuations in the correlations. Thus, a further investigation is needed to better understand the temporal changes in ENSO statistics and their impact on the ENSO-All-India rainfall relationship.

4.3. Wavelet Power Analysis and Coherence

To better understand the non-stationarity of ENSO statistics, the wavelet power spectra associated with the ENSO time series were computed (Figure 6). Enhanced variance in the 16- to 64-month band is seen after 1965 for all the time series. For the Niño 3 and Niño 4 time series, there is also enhanced variance in the 16- to 64-month period band from 1875 to 1895, whereas the enhanced variance persists to around 1905 for the Niño 3.4 time series. Another important aspect of the wavelet power spectra is that the cumulative area-wise significance regions extend across many periods. For example, in the wavelet power spectrum of the Niño 1+2 index, there is a period-elongated region around 1997/1998 extending from a period close to 4 months to a period around 64 months. A similar feature is also evident in the wavelet power spectrum of the Niño 3 and Niño 3.4 indices but appears to be less pronounced in the wavelet power spectrum of the Niño 4 index. The appearance of holes in contoured regions suggests that there are oscillatory modes with nearby frequencies (Schulte, et al., 2015), though the wavelet power spectra cannot determine if there is phase coupling between the oscillatory modes.

The wavelet coherence spectrum shown in Figure 7, indicates that the All-India rainfall relationship with the Niño 1+2 and Niño 4 indices in the 16- to 64-month period band breaks down after 1995, which is consistent with the findings from the sliding correlation analysis shown in Figure 5. The relationship between rainfall and these ENSO indices also weakens around 1925, but this weakening does not appear in the sliding correlation analysis. Note that

~~the lack of coherence after 1995 coincides with the enhanced ENSO variance, implying that higher ENSO variance need not be associated with higher All-India rainfall variance at those time scales. This result implies that intense ENSO events arising from variance in the 16- to 64-month period band need not correspond with unusual monsoon seasons. Indeed, the 1997/1998 ENSO event, which coincides with high power in the 16- to 64-month period band, was associated with a near-normal 1997 monsoon season. More generally, these results imply that the difference Niño 1+2 – AIR is periodic in the 16- to 64-month period band, where AIR is All-India rainfall. The periodic property was confirmed by computing the wavelet power spectrum of Niño 1+2 – AIR (supplementary Figure S2), with the periodicity implying that time periods when ENSO overpredicts and underpredicts rainfall occur in regular intervals. Thus, the result contradicts previous findings suggesting that the relationship between ENSO and Indian rainfall fluctuates randomly (Yun and Timmermann, 2018). In other words, changes in ENSO variance could be contributing to the weakening time-domain correlation. However, ENSO skewness is also enhanced during this time period (Figure 5a) so that weakening relationships may not be simply related to ENSO variance.~~

~~Averaging wavelet coherence in the 16 to 64-month period band further illustrates how the wavelet coherence varies temporally (Figure 8). For example, wavelet coherence with both the ENSO indices reaches approximately 0.8 around 1975 before falling below 0.1 in the mid 1990s. Because the coherence plots shown in Figure 7 are similar, it is difficult to diagnose why the sliding correlation curves shown in Figure 5 have different temporal structures. For example, the period-averaged coherence shown in Figure 8 between rainfall and both the ENSO indices are identical around 1998 yet the relationship between the Niño 1+2 and All-India rainfall is weaker than the relationship between the Niño 4 index and All-India rainfall around that time (Figures 5b and 5c). Thus, a further analysis is needed to extract information unrevealed by the linear wavelet power and coherence methods.~~

To better understand the non-stationarity of ENSO statistics, the wavelet power spectra associated with the ENSO time series were computed (Figure 6). Enhanced variance in the 16- to 64-month band is seen after 1965 for all the time series. For the Niño 3 and Niño 4 time series, there is also enhanced variance in the 16- to 64-month period band from 1875 to 1895, whereas the enhanced variance persists to around 1905 for the Niño 3.4 time series. Another important aspect of the wavelet power spectra is that the cumulative area-wise significance regions extend across many periods. For example, in the wavelet power spectrum of the Niño 1+2 index, there is a period-elongated region around 1997/1998 extending from a period close to 4 months to a period around 64 months. A similar feature is also evident in the wavelet power spectrum of the Niño 3 and Niño 3.4 indices but appears to be less pronounced in the wavelet power spectrum of the Niño 4 index. The appearance of holes in contoured regions suggests that there are oscillatory modes with nearby frequencies (Schulte, et al., 2015), though the wavelet power spectra cannot determine if there is phase coupling between the oscillatory modes.

The wavelet coherence spectrum shown in Figure 7, indicates that the All-India rainfall relationship with the Niño 1+2 and Niño 4 indices in the 16- to 64-month period band breaks down after 1995, which is consistent with the findings from the sliding correlation analysis shown in Figure 5. The relationship between All-India rainfall and these ENSO indices also weakens around 1925, but this weakening does not appear in the sliding correlation analysis. Note that the lack of coherence after 1995 coincides with the enhanced ENSO variance, implying that higher ENSO variance need not be associated with higher All-India rainfall variance at those time scales so that changes in ENSO variance could be contributing to the weakening ENSO-All-India time-domain correlation. However, ENSO skewness is also enhanced during this time period (Figure 4) so that weakening relationships may not be simply related to ENSO variance. Because the coherence plots shown in Figure 7 are similar, it is difficult to diagnose why the sliding correlation curves shown in Figure 5 have different temporal structures. Thus, a further analysis is needed to extract information unrevealed by the linear wavelet power and coherence methods.

~~**4.2. Global Auto-bicoherence**~~

~~**4.2.1 ENSO**~~

~~As a first step for better understanding the All-India rainfall-ENSO correlation curves shown in Figure 5, the global auto-bicoherence spectra associated with the ENSO time series were computed (Figure 9). For all four ENSO~~

metrics, statistically significant auto-bicoherence was identified, with the global auto-bicoherence spectrum of the Niño 1+2 index containing the greatest number of statistically significant auto-bicoherence estimates. A few notable peaks in the Niño 1+2 index auto-bicoherence spectrum are located at (148, 105), (148, 52), (62, 44), and (88, 88) [months]. The auto-bicoherence peak at (88, 88) suggests that there is phase coupling between an 88-month mode (~ 7 years) and a 44-month mode (~ 3.5 years). The auto-bicoherence spectrum of the Niño 3, Niño 3.4, and Niño 4 indices all contain statistically significant auto-bicoherence peaks at (31, 31), implying phase coupling between a 31-month mode and a harmonic with a period of 15.5 months. For the Niño 3.4 index, there is also an on-diagonal peak at (55.6, 55.6), whereas for the Niño 3 index the peak is slightly shifted and located at (62, 44). A third peak in the Niño 3.4 spectrum was found at (105, 47), which could be associated with decadal-scale amplitude modulations of ENSO, though the peak does not correspond to the linkage between the 18-year and 2-year variance identified by Timmermann (2003). The differences among the auto-bicoherence spectra suggests that the nonlinear character of SSTs varies spatially, which is consistent with prior work showing how skewness is generally highest in the eastern equatorial Pacific and lowest in the central equatorial Pacific (An and Jin, 2004).

To confirm the spatial heterogeneity in the nonlinear characteristics of SSTs, the auto-bicoherence associated with SSTs at a few select peaks (p_1, p_2) were computed at each grid point in the domain bounded by 20°N and 20°S and by 146°E and 80°W. The peaks were selected based on the auto-bicoherence spectra of the Niño 3.4 and Niño 1+2 indices. To select the peaks, local maxima in auto-bicoherence within the statistically significance regions shown in Figure 9 were identified.

The spatial structure of auto-bicoherence corresponding to the peaks in the Niño 3.4 auto-bicoherence spectrum are shown in Figure 10. The auto-bicoherence associated with the pair (31, 31) is greatest across the central equatorial Pacific, with the overall spatial pattern being reminiscent of a central Pacific El Niño (Lee and McPhaden, 2010). This result suggests that the phase coupling between the 31-month mode and the 15.5-month mode could be related to the occurrence of central Pacific El Niño events (Section 5). In contrast, the auto-bicoherence pattern associated with the pair (56, 56) is more uniform, with auto-bicoherence slightly greater across the extreme eastern equatorial Pacific than the central equatorial Pacific. This pattern is reminiscent of an eastern Pacific El Niño. Like the pattern corresponding to the pair (31, 31), the auto-bicoherence for the pair (105, 57) tends to be greater across the central equatorial Pacific. Our findings suggest that different nonlinear modes contribute to different ENSO flavors. Although An and Jin (2004) and Burgers and Stephenson (1999) showed that skewness is greatest across the eastern equatorial Pacific, we determined that such a time-domain approach is unable to capture frequency-dependent patterns in nonlinearity.

The spatial auto-bicoherence plots associated with the peaks in the Niño 1+2 auto-bicoherence spectrum are shown in Figure 11. The auto-bicoherence associated with the pairs (148, 53) and (148, 105) is strong across the eastern equatorial Pacific but weak across the central equatorial Pacific, suggesting that the phase coupling between the 148- and 105-month modes and between the 148- and 53-month modes are associated with the skewness of eastern equatorial Pacific SSTs. The pattern associated with the pair (62, 44) is reminiscent of an eastern Pacific El Niño and the auto-bicoherence associated with the pair (88, 88) is relatively weak across the entire equatorial Pacific. A comparison of Figures 10 and 11 shows that there is a tendency for auto-bicoherence to be greater across the eastern equatorial Pacific than the central equatorial Pacific, which is consistent with the results of An and Jin (2004) and Burgers and Stephenson (1999) who found that SSTs across eastern equatorial Pacific are most skewed. The results are also in agreement with Figure 5a, which shows how the magnitude of Niño 1+2 skewness is greater than that of the Niño 4 skewness after the 1970s.

4.2.2 India Rainfall

The global auto-bicoherence spectra for the rainfall time series are shown in Figure 12. For all the rainfall time series except for the central Northeast time series, statistically significant auto-bicoherence was identified. The auto-bicoherence spectrum of the All-India time series contains four on-diagonal peaks, one located around (4,4), another located at (18, 18), and two more located around (40, 40) and (90, 90) [months]. Each of these peaks indicate time series components with periods 4, 18, 40, 90 months are phase-coupled to the corresponding harmonics with periods of 2, 9, 20, and 45 months. Such phase-coupling is inconsistent with the null hypothesis of red noise, which

agrees with the findings of Schulte (2019) who found robust evidence that there are features embedded in the India rainfall time series that exceed a red noise background. Thus, it is natural to ask if these peaks are inherited from a nonlinear climate forcing. For example, the peak (90, 90) in the All India rainfall auto bicoherence spectrum corresponds well with the peak found in the auto bicoherence spectra of the Niño 1+2 time series (Figure 9).

Figure 12 also reveals how the nonlinear characteristics corresponding to each region differ. The statistically significant auto bicoherence for the Peninsula, Northwest, West Central, and Northeast time series is mainly located in regions for which p_1 and p_2 are less than 16 months. However, a peak at (256, 32) was found in the auto bicoherence spectrum of the Northeast time series, suggesting that the time series components with periods 28, 32, and 256 are phase dependent. Many other differences are also seen through an inspection of Figure 12. Our findings suggest that the processes governing precipitation variability in each of the regions differ (Roy and Tedeschi, 2016).

4.3 Local auto-bicoherence

4.3.1 ENSO

To determine if the strength of the identified nonlinearities changes with time, the local diagonal slices corresponding to the global auto bicoherence spectra shown in Figure 9 were computed. The results shown in Figure 13 reveal that the auto bicoherence spectra of all ENSO time series contain statistically significant local auto bicoherence, but the spectrum of the Niño 4 index is only associated with a few statistically significant regions such as the one around 2015 at a period of 32 months.

For the Niño 3 and Niño 3.4 time series, two features of interest are seen in the time period extending from 1973 to 2017 in the 16- to 64 month period band. The first feature is the time elongated region of statistical significance extending from 1973 to 2016 around a period of 61 months. This result implies that after 1973 the nonlinear phase coupling between modes with periods of approximately 30.5 and 61 intensifies. This intensification is consistent with studies showing that ENSO underwent a regime shift in the 1970s in which ENSO began to evolve more nonlinearly than in previous decades (Santoso et al., 2013). This intensification is also evident in the Niño 1+2 auto bicoherence spectrum, though the exact periods associated with the phase coupled oscillatory modes are more difficult to discern. Nevertheless, a comparison of Figures 5a and 13 reveals that enhanced skewness coincides with stronger auto bicoherence in the 32- to 64 month period, suggesting that the skewness partially arose from the stronger phase coupling among modes with periods ranging from 32 to 64 months. The correspondence between auto bicoherence and time domain skewness also holds for the Niño 3 and Niño 3.4 time series (not shown). Our findings suggest that phase coupling among modes embedded in the 32- to 64 month period band plays an important role in generating the skewness of ENSO warm events.

The second feature of interest in Niño 3 and Niño 3.4 auto bicoherence spectra is the one that emerges around 1995 at a period of 31 months. Despite how recent studies indicate that the ENSO regime shift occurred around 1973, this result suggests that the onset of this phase coupling occurred well after the 1970s regime shift just before the 1997/1998 El Niño event. Thus, the nonlinear character of, say, the 1982/1983 El Niño is different from that of both the 1997/1998 and 2015/2016 El Niño events because of the additional phase coupling between the 15.5- and 31 month modes. It is also noted that Figure 13 also shows that there are other time periods when ENSO behaved nonlinearly, and so the recent nonlinear events may not be unique to recent decades. For example, the auto bicoherence spectrum of the Niño 3.4 time series is associated with enhanced auto bicoherence around 1875 in the 32- to 128 month period band. Nevertheless, our findings reveal that the stationarity of the phase coupling in recent decades is unprecedented with respect to any other time period.

To confirm that the nonlinear phase coupling identified in Figure 13 is associated with skewed waveforms, we inspected the corresponding local bi phase spectra (not shown). It was found that the bi phase in the 42- to 64 month period band is generally 0° so that the nonlinear phase coupling in that period band contributes to the positive skewness of the 1982/1983, 1997/1998, and 2015/2016 events.

The temporal change in the auto bicoherence associated with the Niño 1+2 and Niño 4 indices was further illustrated by averaging the local auto bicoherence in the 32- to 64 month period band. As shown in Figure 8, the

auto-bicoherence associated with both ENSO indices increases after the 1970s. This increase in auto-bicoherence coincides with the increase in skewness shown in Figure 5. Thus, the skewness of the Niño 1+2 and Niño 4 indices appears to be related to the auto-bicoherence in the 32- to 64-month period band. It also noted that the auto-bicoherence associated with the Niño 1+2 index peaks around 1998, which is consistent with how the 1997/1998 Niño 1+2 warm event arose from nonlinear processes (An, and Jin, 2004). The auto-bicoherence was also high around the nonlinear event 1982/1983 event (An and Jin, 2004), further supporting the idea that the skewness of individual Niño 1+2 warm events is connected to the nonlinear phase coupling in the 32- to 64-month period band.

Figure 8 shows that the auto-bicoherence spectra of all ENSO time series contain statistically significant local auto-bicoherence, but the spectrum of the Niño 4 index is only associated with a few statistically significant regions such as the one around 2015 at a period of 32 months. For the Niño 3 and Niño 3.4 time series, two features of interest are seen in the time period extending from 1973 to 2016 in the 16- to 64-month period band. The first feature is the time-elongated region of statistical significance extending from 1973 to 2016 around a period of 61 months. This result implies that after 1973 the nonlinear phase coupling between modes with periods of approximately 30.5 and 61 intensifies. This intensification is consistent with studies showing that ENSO underwent a regime shift in the 1970s in which ENSO began to evolve more nonlinearly than in previous decades (Santoso et al., 2013). This intensification is also evident in the Niño 1+2 auto-bicoherence spectrum, though the exact periods associated with the phase-coupled oscillatory modes are more difficult to discern. Nevertheless, a comparison of Figures 4 and 8 reveals that enhanced skewness coincides with stronger auto-bicoherence in the 32- to 64-month period, suggesting that the skewness partially arose from the stronger phase coupling among modes with periods ranging from 32 to 64 months. The correspondence between auto-bicoherence and time-domain skewness also holds for the Niño 3 and Niño 3.4 time series (not shown).

The second feature of interest in the Niño 3 and Niño 3.4 auto-bicoherence spectra is the one that emerges around 1995 at a period of 31 months. Despite how recent studies indicate that the ENSO regime shift occurred around 1973, this result suggests that the onset of this phase coupling occurred well after the 1970s regime shift just before the 1997/1998 El Niño event. Thus, the nonlinear character of, say, the 1982/1983 El Niño is different from that of both the 1997/1998 and 2015/2016 El Niño events because of the additional phase coupling between the 15.5- and 31-month modes. It is also noted that Figure 8 also shows that there are other time periods when ENSO behaved nonlinearly, and so the recent nonlinear events may not be unique to recent decades. For example, the auto-bicoherence spectrum of the Niño 3.4 time series is associated with enhanced auto-bicoherence around 1875 in the 32- to 128-month period band. Nevertheless, our findings reveal that the stationarity of the phase coupling in recent decades is unprecedented with respect to any other time period.

To confirm that the nonlinear phase coupling identified in Figure 8 is associated with skewed waveforms, we inspected the corresponding local bi-phase spectra (not shown). It was found that the bi-phase in the 42- to 64-month period band is generally 0° so that the nonlinear phase coupling in that period band contributes to the positive skewness of the 1982/1983, 1997/1998, and 2015/2016 events.

~~**4.3.2 Local Bicoherence of India Rainfall and Non-linear Coherence**~~

4.4 Nonlinear Coherence between All-India Rainfall and ENSO

~~The local auto-bicoherence spectra of the India rainfall time series are shown in Figure 14. The statistically significant auto-bicoherence was identified for all six time series, mainly for periods less than 64 months. The results suggest that the phase-coupling is many among higher-frequency modes. However, for the All-India rainfall time series, the auto-bicoherence spectrum reveals two time periods of statistically significant auto-bicoherence in the 64- to 128-month period band. The first region extends from 1885 to 1925 and the second region extends from 1945 to around 1985. The nonlinearities found in the India rainfall auto-bicoherence spectra were also found to be cumulative arc-wise significant, though some differences in the results were found (Figure S3 in supplementary material). The statistical significance of the results was further checked using the topological significance test (Schulte, 2019), which also provided evidence that the time series are nonlinear (Figure S4 supplementary material).~~

~~To determine if the nonlinearities identified for All-India rainfall is related to ENSO, nonlinear coherence was computed along the local diagonal slices of the auto-bicoherence spectra for both All-India rainfall and the four ENSO metrics considered in this study. Furthermore, All-India rainfall is generally more strongly coherent with ENSO than rainfall associated with the individual rainfall regions (Schulte, 2019) so only the results for All-India rainfall are shown for brevity.~~

~~The results shown in Figure 15 indicate that the nonlinear wavelet coherence between All-India rainfall and the time series for the all four ENSO indices is statistically significant in the 32- to 64-month period band. The nonlinear coherence in this period band appears to peak around the 1972/1973 El Niño event, indicating that an increase in positive skewness of ENSO should tend to coincide with enhanced negative skewness of All-India rainfall around this time. As shown in Figure 8, the nonlinear coherence averaged in the 32- to 64-month period band fluctuates less than linear coherence and reaches a clear global maximum around 1972/1973 before rapidly declining to a global minimum around the 1997/1998 El Niño event when the Niño 1+2 index is very nonlinear (Figures 8 and 13). Therefore, according to the discussion in Section 3.5, changes in ENSO skewness contributed to the weakening relationships between ENSO and All-India rainfall shown in Figures 5a and 5b.~~

The results shown in Figure 9 indicate that the nonlinear wavelet coherence between All-India rainfall and the time series for the all four ENSO indices is statistically significant in the 32- to 64-month period band mainly prior to the 1980s. The nonlinear coherence in this period band appears to peak around the 1972/1973 El Niño event, indicating that an increase in positive skewness of ENSO should tend to coincide with enhanced negative skewness of All-India rainfall around this time. However, much of the statistically nonlinear coherence is located during the time period when ENSO is more linear than it has been in recent decades (Figure 8) so that the effects of nonlinearities will be small regardless of the nonlinear wavelet coherence. In contrast, the auto-bicoherence of the ENSO time series in the 32- to 64-month period band is statistically significant and high after the 1970s (Figure 8) so that lack of nonlinear coherence after 1980s shown in Figure 9 is expected to impact the time-domain correlation more strongly, much like the theoretical situation shown in Figure 2. Our results are consistent with this theoretical idea because the Niño 1+2-All-India rainfall relationship weakens more than the Niño 4-All-India rainfall relationship after the 1970s (Figure 5), which is expected because the Nino 1+2 index is more nonlinear than the Nino 4 index during this time period. However, unlike the theoretical example shown in Figure 2, the linear coherence between the ENSO time series and All-India rainfall also weakens around the 1990s (Figure 8) so that the weakening relationship could be the result of a combination of factors that includes ENSO nonlinearity.

The 20-year sliding mean of the ENSO auto-bicoherence, coherence, and nonlinear coherence averaged in the 32 to 64-month period band further highlights the impact of ENSO nonlinearity. As shown in Figure 10a, the sliding mean nonlinear coherence between the Niño 1+2 index and All-India rainfall fluctuates less than linear coherence and reaches a clear global maximum around the 1970s before rapidly declining to a global minimum around the late 1990s when the Niño 1+2 index is very nonlinear. As shown in Figure 10a, the Niño 1+2 auto-bicoherence peaks around the same time the August-September Niño 1+2-All-India rainfall correlation is weakest. In fact, the correlation between the sliding September-August Niño 1+2-All-India rainfall correlation time series and the sliding Nino 1+2 auto-bicoherence time series is 0.81, much higher than the correlation with linear coherence ($r = -0.11$) and nonlinear coherence ($r = -0.34$). These results support the idea that the Nino 1+2 regime shift impacted the weakening time-domain correlation. On the other hand, the correlation between Niño 4 auto-bicoherence and the August-September Niño 4-All-India correlation time series is weak so that changes in the nonlinearity of the Niño 4 index unlikely contributed to changes in the Niño 4-All-India rainfall relationship. Nevertheless, this result agrees with theory that suggests that nonlinearity is only an important contributor when the timeseries is highly nonlinear, which is not the case for the Niño 4 index because of the low auto-bicoherence (Figure 10b). Thus, not all the weakening in the ENSO-All-India rainfall relationship can be attributed to ENSO nonlinearity. However, because the nonlinear coherence between All-India rainfall and indices for the Niño 1+2 and Niño 4 is weak (Figure 10), the more pronounced weakening in the August-September Nino 1+2-All-India rainfall correlation reflects the more intense increase in Niño 1+2 nonlinearity compared to that of the Niño 4 index in recent decades.

4.5. A possible explanation for the weakening

To better understand the association between ENSO nonlinearity and the All-India rainfall-ENSO relationship, the global auto-bicoherence spectra associated with the ENSO time series were first computed (Figure 11). Then, the auto-bicoherence of SSTs associated with a few select peaks (p_1, p_2) in Figure 8 were computed at each grid point in the domain bounded by 20°N and 20°S and by 146°E and 80°W. The peaks were selected based on the auto-bicoherence spectra of the Niño 3.4 and Niño 1+2 indices. To select the peaks, local maxima in auto-bicoherence within the statistically significance regions shown in Figure 11 were identified, where points associated with local maxima were chosen because they were associated with the clearest patterns.

The spatial structure of auto-bicoherence corresponding to the peaks in the Niño 3.4 auto-bicoherence spectrum are shown in Figure 12. The auto-bicoherence associated with the pair (31, 31) is greatest across the central equatorial Pacific, with the overall spatial pattern being reminiscent of a central Pacific El Niño (Lee and McPhaden, 2010). This result suggests that the phase coupling between the 31-month mode and the 15.5-month mode could be related to the occurrence of central Pacific El Niño events (Section 5). In contrast, the auto-bicoherence pattern associated with the pair (56, 56) is more uniform, with auto-bicoherence slightly greater across the extreme eastern equatorial Pacific than the central equatorial Pacific. This pattern is reminiscent of an eastern Pacific El Niño. Like the pattern corresponding to the pair (31, 31), the auto-bicoherence for the pair (105, 57) tends to be greater across the central equatorial Pacific. Our findings suggest that different nonlinear modes contribute to different ENSO flavors. Although An and Jin (2004) and Burgers and Stephenson (1999) showed that skewness is greatest across the eastern equatorial Pacific, we determined that such a time-domain approach is unable to capture frequency-dependent patterns in nonlinearity.

The spatial auto-bicoherence plots associated with the peaks in the Niño 1+2 auto-bicoherence spectrum are shown in Figure 13. The auto-bicoherence associated with the pairs (148, 53) and (148, 105) is strong across the eastern equatorial Pacific but weak across the central equatorial Pacific, suggesting that the phase coupling between the 148- and 105-month modes and between the 148- and 53-month modes are associated with the skewness of eastern equatorial Pacific SSTs. The pattern associated with the pair (62, 44) is reminiscent of an eastern Pacific El Niño and the auto-bicoherence associated with the pair (88, 88) is relatively weak across the entire equatorial Pacific. A comparison of Figures 12 and 13 shows that there is a tendency for auto-bicoherence to be greater across the eastern equatorial Pacific than the central equatorial Pacific, which is consistent with the results of An and Jin (2004) and Burgers and Stephenson (1999) who found that SSTs across eastern equatorial Pacific are most skewed. The results are also in agreement with Figure 4a which shows how the magnitude of Niño 1+2 skewness is greater than that of the Niño 4 skewness after the 1970s.

5. Discussion/Conclusion

The nonlinear nature of both ENSO and Indian rainfall were examined using higher-order wavelet methods. The auto-bicoherence spectra of the four ENSO time series revelated that ENSO skewness arose from the phase coupling of modes with various periods. The Niño 3.4 time series was found to contain coupling between modes with period 31 and 15.5 in addition to coupling between modes with period of 61 months and 30.5 months. The phase-coupling between the 31 and 15.5 modes was found to be especially strong after 1995, whereas the phase coupling between the 61- and 30.5-month modes was found to intensify after the 1970s. The stronger phase coupling after the 1970s is consistent with how ENSO underwent a regime shift in the 1970s (Santoso et al., 2013), which was marked by an increase in ENSO skewness.

The evolution of SSTs across the Niño 4, Niño 3.4, Niño 3, and Niño 1+2 regions was found to be nonlinear, but the degree to which the time series are nonlinear are different. Overall, the Niño 1+2 time series was found to be the most nonlinear, while the Niño 4 index was found to be the most linear. The spatial patterns associated with the nonlinearities depend on the frequency components contributing to the nonlinearities. For example, phase coupling between the modes with periods of 31 and 15.5 months was found to be strongest in the central equatorial Pacific and weakest across the eastern equatorial Pacific. This finding suggest that the occurrence of central Pacific El Niño events could be linked to this phase coupling, which is relevant to understanding the Indian monsoon because central Pacific El Nino events have been shown to be more effective at creating drought-inducing subsidence over India (Kumar et al., 2006).

The results from the present and previous studies (Fan et al. 2017) supports the idea that changes in the ENSO-India rainfall relationship are related to ENSO flavors because ENSO nonlinearity appears to be related to ENSO flavors (Figures 10 and 11), opposing the findings of other work showing that the changes are related to sampling variability or to noise. According to Yun and Timmermann (2018), the changes in the time-domain correlation between All-India summer rainfall (ISMR) and ENSO is consistent with the assumption that ISMR is the sum of the ENSO signal and Gaussian white noise (i.e., ISMR = ENSO + white noise). ~~However, for this hypothesis to hold, the difference ISMR – ENSO must be Gaussian white noise. As shown in this study, the nonlinear wavelet coherence between ENSO metrics and All-India rainfall is weak, which means that the difference ISMR – ENSO will have non-Gaussian noise features so that ISMR is not consistent with a stochastically perturbed ENSO signal. The retention of non-Gaussian noise features is certainly the case for $R(t) - F(t)$ in the example in Section 3.5 because the difference would retain the cosine function with a period of 16. In the case of ISMR, the lack of nonlinear coherence results in periodic behavior of ENSO – ISMR, which means that Indian rainfall is not simply a stochastically perturbed ENSO signal, as noise does not contain periodicities. In contrast, if ISMR and ENSO were highly nonlinear wavelet coherent, then they would have the same frequency components contributing to skewness and the difference of the two would remove the skewness. Although our results cannot preclude noise as a contributor to fluctuations in the time-domain correlation, the periodic nature of ENSO – ISMR does suggest that monsoon forecast error for a forecast based on ENSO may be predictable to some extent.~~ However, for this hypothesis to hold, the difference ISMR – ENSO must be Gaussian white noise. As shown in this study, the nonlinear wavelet coherence between ENSO metrics and AIR is weak so that ENSO – AIR contains periodicities (Figure S2), which means that AIR is not simply a stochastically perturbed ENSO signal, as noise does not contain periodicities. The retention of non-Gaussian noise features was certainly the case for $R(t) - F(t)$ in the example in Section 3.5 because the difference would retained the cosine function with a period of 16.

The fact that nonlinear coherence between rainfall and ENSO is determined by linear coherence between ENSO and rainfall at two or three frequencies means that the changing time-domain correlation could be more fully understood by determining why linear coherence changes at the frequencies that contribute to ENSO skewness. Such an analysis could provide a more mechanistic perspective than the theoretical perspective adopted in this study. A preliminary analysis showed that enhanced linear coherence between the North Atlantic Oscillation index and All-India rainfall after 1995 in the 16- to 64-month period band associated with ENSO nonlinearity. This result suggests that conditions across the North Atlantic (Kakade, 2000, Bhatla, 2016) could influence the nonlinear coherence between ENSO and All-India rainfall and thus the corresponding time-domain correlation.

~~The higher-order wavelet analysis conducted in this study also revealed that the nonlinear nature of the rainfall time series for the regions considered varied. Our results are consistent with the findings from previous work showing how the physical mechanisms governing precipitation variability are different (Roy and Tedisch, 2016). However, the higher-order wavelet analysis conducted in this study allowed us to determine the time scales on which the rainfall times series features differ. Further research is needed to fully understand why the nonlinear characteristics differ from one region to another. Future work could include conducting nonlinear coherence analyses between indices of various climate modes and the rainfall times series for each region individually.~~

~~A few other possible physical mechanisms behind the nonlinearity of the rainfall time series were examined. For example, we computed the auto-bicoherence spectrum of the IOD and sunspot time series because they have been postulated as climate drivers of Indian Rainfall (Ashok et al., 2001; Ashok et al., 2004; van Loon and Meehl, 2012). Although these time series were found to be highly nonlinear, the auto-bicoherence spectra of them did not correspond well with the rainfall time series. We found that the IOD contains strong coupling between the modes with periods of 256- and 128-months and between modes with periods of 128-months and 64-months (Figures S5 and S6 in supplementary material), but no such coupling was found for any of the rainfall time series. Similarly, the sunspot cycle time series was associated with strong coupling between 128- and 256-month modes (Figures S7 and S8 in supplementary material) but again no such coupling was identified in the rainfall time series. Future work could thus include better understanding the physical mechanisms underlying the nonlinearities identified in this study.~~

The tools used and developed in this study may have important applications in understanding how forecasting systems replicate Indian rainfall and its associated teleconnections. These methods, for example, could determine if forecasting systems can reproduce nonlinear characteristics of climate time series. As such, a R software package has been developed to implement these methods (available at:) ~~T~~hese methods ~~identifications~~ could provide new directions for improving current forecasting systems and ultimately predictions of Indian rainfall.

Appendix A

The first step (STEP 1) in assessing the cumulative-area significance of a point was the calculation of the $N = 12$ sets

$$P_{pw}^{i} = \{(b,a): \rho_{pw}(b,a) < \alpha_i\}, \quad \text{(A1)}$$

where each set is the subset of the wavelet domain consisting of points whose wavelet quantities are point-wise statistically significant at the α_i significance level. In this paper, $\alpha_1 = 0.02$, $\alpha_{12} = 0.18$, and $\alpha_{i+1} - \alpha_i = 0.02$. In the second step (STEP 2), a geometric pathway about x was computed, where a geometric pathway is a nested sequence

$$P_1^x \subseteq P_2^x \subseteq \cdots \subseteq P_N^x \quad \text{(A2)}$$

such that the

$$P_i^x = \{(b,a): (b,a) \in P_{pw}^{i}, (b,a) \sim x\} \quad \text{(A3)}$$

are path-components of P_{pw}^{i} containing x. The equivalence relation $\sim$ on P_{pw}^{i} makes two points in P_{pw}^{i} equivalent if they can be connected by a continuous path in P_{pw}^{i}. The third step (STEP 3) involved the calculation of the normalized area corresponding to P_i^x. The normalized area is defined as patch area divided by the square of mean scale coordinate of the patch, where A_i^x was assumed to be 0 if $P_{pw}^{i} = \phi$ or $P_{pw}^{i} = \{x\}$. The critical area A_i^{crit} was obtained by computing the $(1 - \alpha_c)$th percentile of the null distribution of normalized areas corresponding to the significance level α_i, where α_c is the significance level of the cumulative area-wise test. The null distributions were constructed by generating 1000 patches at the α_i significance level under the null hypothesis of red noise. More specifically, realizations of a red-noise process with lag-1 autocorrelation coefficients equal to that of input time series were used to create the wavelet spectra from which the 1000 patches were obtained. The length of the realizations was set to 200, though the length is irrelevant because patch area is not related to time series length but to the reproducing kernel of the analyzing wavelet (Schulte 2019). The final step (Step 4) was to compute

$$r^x = \frac{1}{N}\sum_{j=1}^{N} \lambda_j^x, \quad \text{(A4)}$$

where $\lambda_j^x = 2$ if $P_j^x / A_j^{crit} > 1$, $\lambda_j^x = 0$ if $P_j^x / A_j^{crit} <= 1$, and A_j^{crit} is the critical area associated with α_j. The wavelet quantity at the point x was deemed statistically significant at the α_c cumulative area-wise level if $r^x > 1$.

Appendix B

For $p > 1$, the $(p+1)$-th order poly spectrum of a time series X is given by

$$B_n^X(s_1, s_2, \dots, s_p) = \widehat{W}_n^X(s_{p+1})\left(\prod_{k=1}^{p} W_n^X(s_k)\right) \quad \text{(B1)}$$

where

$$\frac{1}{s_{p+1}} = \sum_{k=1}^{p} \frac{1}{s_k} \quad \text{(B2)}$$

The third-order poly spectrum is the bi-spectrum, and the fourth-order poly spectrum is the tri-spectrum (Collis et al., 1998), which identifies the frequency components contributing to kurtosis. The $(p+1)$-th order coherence between two time series is given as

$$R_n^2(s) = \frac{\left|S s_{smoth}^{-1} B_n^{XY}(s_1, s_2, \dots, s_p)\right|^2}{S\left(s_{smoth}^{-1}\left|B_n^X(s_1, s_2, \dots, s_p)\right|^2\right) S\left(s_{smoth}^{-1}\left|B_n^Y(s_1, s_2, \dots, s_p)\right|^2\right)}, \quad \text{(B3)}$$

where $B_n^{XY}(s_1, s_2, \dots, s_p)$ is the $(p+1)$-th-order cross-spectrum given by

$$B_n^{XY}(s_1, s_2, \dots, s_p) = B_n^X(s_1, s_2, \dots, s_p)\hat{B}_n^Y(s_1, s_2, \dots, s_p). \quad \text{(B4)}$$

When $p = 2$, Eq. (B3), measures the local cross-correlation between skewness, and when $p = 3$ the equation measures the local cross-correlation between kurtosis.

References

An, S.-I., and Jin, F.-F: Nonlinearity and asymmetry of ENSO., J. Climate, 17, 2399–2412, 2004.

An, S.-I., Ham, Y. G., Kug, J. S., Jin, F.-F., and Kang, I.: El Nino-La Nina asymmetry in the coupled model intercomparison project simulations, J. Climate, 18, 2617-2627, 2005.

An, S-I.: Interdecadal changes in the El Niño-La Niña symmetry, Geophys Res. Lett., 31, L23210, doi:10.1029/2004GL021699, 2004.

An, S.-I.: A review of interdecadal changes in the nonlinearity of the El Nino–Southern Oscillation, Theor. Appl. Climatol., 97, 29–40, 2009.

Ashok, K., Guan, Z., and Yamagata, T.: Impact on the Indian Ocean dipole on the relationship between the Indian monsoon rainfall and ENSO, Geophys Res. Lett., 28, 4499–4502, 2001.

Ashok, K, Guan, Z, Saji, N. H., and Yamagata, T.: Individual and combined influences of ENSO and the Indian Ocean dipole on the Indian summer monsoon, J. Climate, 17, 3141–3155, 2004.

Bhatla, R., Singh, A. K., Mandal, B., Ghosh, S., Pandey, S. N., and Abhijit, S.: Influence of North Atlantic Oscillation on Indian Summer Monsoon Rainfall in Relation to Quasi-Binneal Oscillation, Pure and Applied Geophysics, 173, 2959-2970, 2016.

Blanford, H. F.: On the connexion of the Himalaya snowfall with dry wind and seasons of drought in India, Proc R Soc Lond., 37, 3–22, 1884.

Burgers, G., and Stephenson, D. B: The 'Normality' of ENSO, Geophys Res. Lett., 26, 1027–1030, 1999.

Carey, S. K., Tetzlaff, D., Buttle, J., Laudon, H., McDonnell, J,. McGuire, K., Seibert, J., Soulsby, C., Shanley, J. : Use of color maps and wavelet coherence to discern seasonal and inter annual climate influences on streamflow variability in northern catchments. Water Resources Research, 49, 6194–6207, 2013.

Cash, B. A., Barimalala, R., Kinter, J. L., Altshuler, E. L., Fennessy, M. J., Manganello, J.V., Molteni, F., Towers, P., Vitart, F.: Sampling variability and the changing ENSO–monsoon relationship, Clim. Dyn., 48, 4071–4079, 2017.

Chen, W., Dong, B., and Lu, R.: Impact of the Atlantic Ocean on the multidecadal fluctuation of El Niño-Southern Oscillation-South Asian monsoon relationship in a Coupled General Circulation Model, Journal of Geophysical Research, 115, D17109, https://doi.org/10.1029/2009JD013596, 2010.

Collis, W. B., White, P. R., and Hammond, J. K.: Higher-order Spectra: The Bispectrum and Trispectrum, Mech. Syst. Signal Pr., 12, 375–394, 1998.

Dortch, J. M., Owen, L. A., Haneberg, W. C., Caffee, M. W., Dietsch, C., and Kamp, U.: Nature and timing of large landslides in the Himalaya and Transhimalaya of northern India, Quaternary Science Reviews, 28, 1037-1054, 2009.

Duan, W., Huang, C., Xu, H.: Nonlinearity modulating intensities and spatial structures of central Pacific and eastern Pacific El Niño events, Adv Atmos Sci., 34, 737–756, 2017.

DelSole, T., and Shukla, J.: Climate models produce skillful predictions of Indian summer monsoon rainfall, Geophys Res. Lett, 39, L09703, https://doi.org/10.1029/2012GL051279, 2012.

Elsayed, M. A. K.: Wavelet Bicoherence Analysis of Wind–wave Interaction, Ocean Eng., 33, 458–470, 2006.

Fagan, B.: Floods, famines, and emperors: El Niño and the fate of civilizations, Basic Books, 2009.

Fan, F., Dong, X., Fang, X., Xue, F., Zheng, F., and Zhu, J.: Revisiting the relationship between the south Asian summer monsoon drought and El Niño warming pattern, Atmospheric Sci. Lett., 18, 175–182, 2017.

Gershunov, A., Schneider, N., and Barnett, T.: Low-frequency modulation of the ENSO-Indian monsoon rainfall relationship: Signal or noise?, J. Climate, 14, 2486–2492, 2001.

Grinsted, A., Moore, J. C., and Jevrejeva, S.: Application of the Cross Wavelet Transform and Wavelet Coherence to Geophysical Time Series, Nonlinear Proc. Geophys., 11, 561–566, 2004.

Holman, I. P., Rivas-Casado, M., Bloomfield, J.P., Gurdak, J. J.: Identifying nonstationary groundwater level response to North Atlantic ocean–atmosphere teleconnection patterns using wavelet coherence. Hydrogeol. J. http://dx.doi.org/10.1007/s10040-011-0755-9, 2011.

Hu, S. and Fedorov, A. V.: The extreme El Nino of 2015–2016 and the end of global warming hiatus, Geophys. Res. Lett., 4415 3816–24, 2017

Jin, F.-F., An, S-I., Timmermann, A., and Zhao, J.: Strong El Nino events and nonlinear dynamical heating, Geophys. Res. Lett., 30, 1120, doi:10.1029/2002GL016356, 2003.

Johnson, N.C.: How Many ENSO Flavors Can We Distinguish?, J. Climate, 26, 4816–4827, 2013.

Johnson N. C., and Kosaka, Y.: The role of eastern equatorial Pacific convection on the diversity of boreal winter El Niño teleconnection patterns, Clim. Dyn., 47, 3737–3765, 2016.

Johnson, S. J., Turner, A., Woolnough, S., Martin, G., and MacLachlan, C.: An assessment of Indian monsoon seasonal forecasts and mechanisms underlying monsoon interannual variability in the Met Office GloSea5-GC2 system. Climate Dynamics, 48(5-6), 1447-1465, 2017.

Kakade, S. B., and Dugam, S. S.: The simultaneous effect of NAO and SO on the monsoon activity over India, Geophys Res Lett., 27, 3501–3504, 2000.

Kale, V. : On the link between extreme floods and excess monsoon epochs in South Asia, Climate dynamics, 39, 1107-1122, 2012.

Kalnay, E., and Dalcher, A.: Forecasting forecast skill., Mon. Wea. Rev.,115, 349–356, 1987.

Kang, I.-S., and Kug, J-S.: El Nino and La Ni ~ na sea surface ~ temperature anomalies: Asymmetry characteristics associated with their wind stress anomalies, J. Geophys. Res., 107, 4372, doi:10.1029/2001JD000393, 2002.

Kestin, T. A., Karoly, D. J., Yano, J.-I., and Rayner, N. A.: Time– frequency variability of ENSO and stochastic simulations, J. Climate, 11, 2258–2272, 1998.

King, T.: Quantifying Nonlinearity and Geometry in Time Series of Climate, Quaternary Sci. Rev., 15, 247–266, 1996.

Kripalani, R. H., and Kulkarni, A.: Climatic impact of El Nino/La Nina on the Indian monsoon: A new perspective, Weather, 52, 39-46, 1997.

Kucharski, F., Bracco, A., Yoo, J. H., and Molteni, F.: Low-frequency variability of the Indian monsoon–ENSO relationship and the tropical Atlantic: The "weakening" of the 1980s and 1990s, J. Climate., 20, 4255–4266, 2007.

Kucharski, F., Bracco, A., Yoo, J. H., Tompkins, A. M., Feudale, L., Ruti, P., and Dell'Aquila, A.: A gill-Matsuno-type mechanism explains the tropical Atlantic influence on African and Indian monsoon rainfall, Quarterly Journal of the Royal Meteorological Society, 135, 569–579, 2009.

Kumar, K. K., Soman, M. K., and Kumar, K. R.: Seasonal forecasting of Indian summer monsoon rainfall: a review, Weather, 50, 449-467, 1995

Krishnamurthy, V., and Goswami, B. N.: Indian monsoon–ENSO relationship on interdecadal timescale, J. Climate, 13, 579–595, 2000.

Kripalani, R. H., and Kulkarni, A.: Climatic impact of El Nino/ La Nina on the Indian monsoon: A new perspective, Weather, 52, 39–46, 1997.

Kumar, K. K., Rajagopalan, B., and Cane, M. A.: On the weakening relationship between the Indian monsoon and ENSO, Science, 284, 2156–2159, 1999.

Kumar, K. K., Rajagopalan, B., Hoerling, M., Bates, G., Cane, M. A.: Unraveling the Mystery of Indian Monsoon Failure During El Niño, Science, 314, 115-119, 2006.

Lee, T., and McPhaden, M. J.: Increasing intensity of El Niño in the central-equatorial Pacific, Geophys. Res. Lett., 37, L14603, doi: 10.1029/2010GL044007, 2010.

Lu, R., Dong, B., and Ding, H.: Impact of the Atlantic Multidecadal Oscillation on the Asian summer monsoon, Geophys. Res. Lett., 33, L24701, https://doi.org/10.1029/2006GL027655, 2006.

McPhaden, M. J.: Genesis and evolution of the 1997–98 El Nino, Science, 283, 950–954, 1999.

Maccarone, T. J.: The Biphase Explained: Understanding the Asymmetries in Coupled Fourier Components of Astronomical Timeseries, Mon. Not. R. Astron. Soc., 435, 3547, doi:10.1093/mnras/stu1824, 2013.

Maraun, D.,and Kurths, J.: Cross wavelet analysis: significance testing and pitfalls. Nonlinear Process. Geophys., 11, 505–514., 2004.

Maraun, D., Kurths, J., and Holschneider, M.: Nonstationary Gaussian Processes in the Wavelet Domain: Synthesis, Estimation, and Significance Testing, Phys. Rev. E, 75, 016707, doi:10.1103/PhysRevE.75.016707, 2007.

Mishra, V., Aadhar, S., Asoka, A., Pai, S., & Kumar, R.: On the frequency of the 2015 monsoon season drought in the Indo-Gangetic Plain, Geophysical Research Letters, 43, 12-102, 2016.

Munot, A. A., and Kumar, K. K.: Long range prediction of Indian summer monsoon rainfall. Journal of earth system science, 116, 73-79, 2007.

Ng, E. K. W. and Chan, J. C. L.: Geophysical applications of partial wavelet coherence and multiple waveletcoherence, J. Atmos. Ocean. Tech., 29, 1845–1853, 2012.

Parthasarathy, B., Munot, A. A., and Kothawale, D. R.: Regression model for estimation of Indian foodgrain production from summer monsoon rainfall, Agricultural and Forest Meteorology, 42, 167-182, 1988.

Parthasarathy, B., Munot, A. A., and Kothawale, D. R.: All-India monthly and seasonal rainfall series: 1871–1993, Theoretical and Applied Climatology, 49, 217–224. 1994.

Pokhrel, S., Saha, S. K., Dhakate, A., Rahman, H., Chaudhari, H. S., Salunke, K.,Hazra, A., Sujith, K., Sikka, D. R.: Seasonal prediction of Indian summer monsoon rainfall in NCEP CFSv2: forecast and predictability error, Climate dynamics, 46, 2305-2326, 2016.

Prasanna, V. (2014). Impact of monsoon rainfall on the total foodgrain yield over India. *Journal of earth system science*, *123*(5), 1129-1145, 2014.

Rajeevan, M., Pai, D. S., Kumar, R. A., and Lal, B.: New statistical models for long-range forecasting of southwest monsoon rainfall over India, Climate Dynamics, 28, 813-828, 2007.

Rayner, N. A., Parker, D. E., Horton, E. B., Folland, C. K., Alexander, L. V., Rowell, D. P., Kent, E. C., and Kaplan, A.: Global analyses of sea surface temperature, sea ice, and night marine air temperature since the late nineteenth century, J. Geophys. Res., 108, 4407, doi: 10.1029/2002JD002670,2003.

Ropelewski, C. F, Halpert ,M. S. : Global and regional scale precipitation patterns associated with the El Niño/Southern Oscillation., Monthly Weather Review, 115, 1606–1626, 1987.

Roy, I. and Tedeschi, R. G.: Influence of ENSO on regional indian summer monsoon precipitation—local atmospheric influences or remote influence from pacific, Atmosphere, 7, 25, 2016.

Santoso, A., McGregor, S., Jin, F.-F., Cai, W., England, M. H., An, S.-I., McPhaden, M. J., and Guilyardi, E.: Late-twentieth-century emergence of the El Niño propagation asymmetry and future projections., Nature, 504, 126–130, 2013.

Santoso, A., McPhaden, M. J., Cai, W.: The defining characteristics of ENSO extremes and the strong 2015/2016 El Niño, Rev. Geophys, 55, 1079–1129, 2017.

Sanyal, J., and Lu, X. X.: Remote sensing and GIS-based flood vulnerability assessment of human settlements: a case study of Gangetic West Bengal, India. Hydrological Processes: An International Journal, 19, 3699-3716, 2005.

Schaefli, B., Maraun, D., and Holschneider, M.: What drives high flow events in the Swiss Alps? Recent developments in wavelet spectral analysis and their application to hydrology, Adv. Water Resour., 30, 2511–2525, 2007.

Schulte, J. A.: Statistical hypothesis testing in wavelet analysis: theoretical developments and applications to Indian rainfall, Nonlin. Processes Geophys., 26, 91-108, https://doi.org/10.5194/npg-26-91-2019, 2019.

Schulte, J. A.: Cumulative areawise testing in wavelet analysis and its application to geophysical time-series, Nonlin. Processes Geophys., 23, 45-57, 2016.

Schulte, J. A.: Wavelet analysis for non-stationary, nonlinear time series, Nonlin. Processes Geophys., 23, 257-267, https://doi.org/10.5194/npg-23-257-2016, 2016.

Schulte, J. A., Duffy, C., and Najjar, R. G.: Geometric and Topological Approaches to Significance Testing in Wavelet Analysis, Nonlin. Processes Geophys., 22, 139-156, 2015.

Shen, X., and Kimoto, M.: Influence of El Niño on the 1997 Indian summer monsoon, J. Meteor. Soc. Japan, 77, 1023–1037, 1999.

Shukla, J., and Paolino, D. A.: The Southern Oscillation and long-range forecasting of the summer monsoon rainfall over India. Monthly Weather Review, 111, 1830-1837, 1983.

Slingo, J. M., and Annamalai, H.: 1997: The El Niño of the century and the response of the Indian summer monsoon, Mon. Wea. Rev., 128, 1778–1797, 2000.

Timmermann, A.: Decadal ENSO amp_litude modulations: A nonlinear mechanism, Global Planet. Change, 37, 135–156, 2003.

Torrence, C., and Webster, P. J.: Interdecadal changes in the ENSO-monsoon system, J. Climate, 12, 2679–2690. 1999.

Van Milligen, B. P., Saìnchez, E., Estrada, T., Hidalgo, C., Brañas,B., Carreras, B., and Garcìa, L.: Wavelet Bicoherence: A New Turbulence Analysis Tool, Phys. Plasmas, 2, 3017–3032, 1995.

Walker, G. T., and Bliss, E. W.: World weather V, Mem., R. Meteorol. Soc., 4, 53–84, 1932.

Wu, A., and Hsieh, W. W.: Nonlinear interdecadal changes of the El Niño-Southern Oscillation, Climate Dyn., 21, 719–730, 2003.

Yun, K. S and Timmermann, A.: Decadal monsoon-ENSO relationships reexamined, Geophys Res Lett., 45, 2014–2021, 2018.

Zhang, Q., Xu, C., Jiang, T., Wu, Y.: Possible influence of ENSO on annual maximum streamflow of the Yangtze River, China, Journal of Hydrol, 333, 265–274. doi:10.1016/ j.jhydrol.2006.08.010, 2007

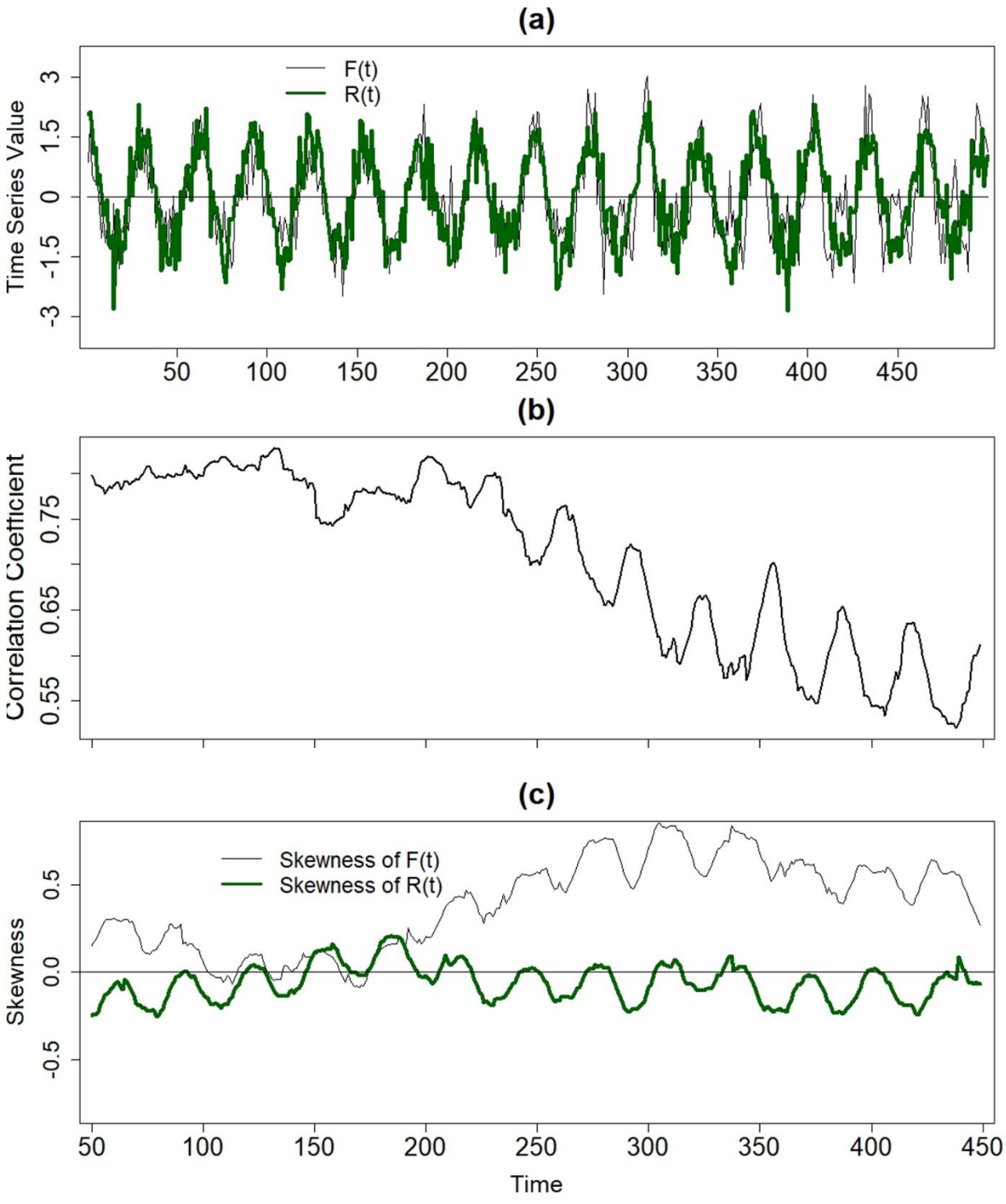

1332

1333 Figure 1. (a) An idealized nonlinear forcing time series together with an idealized response *R*(*t*). The 120-
1334 point sliding correlation between *F*(*t*) and *R*(*t*). (c) The 120-point sliding skewness of *F*(*t*) and *R*(*t*).

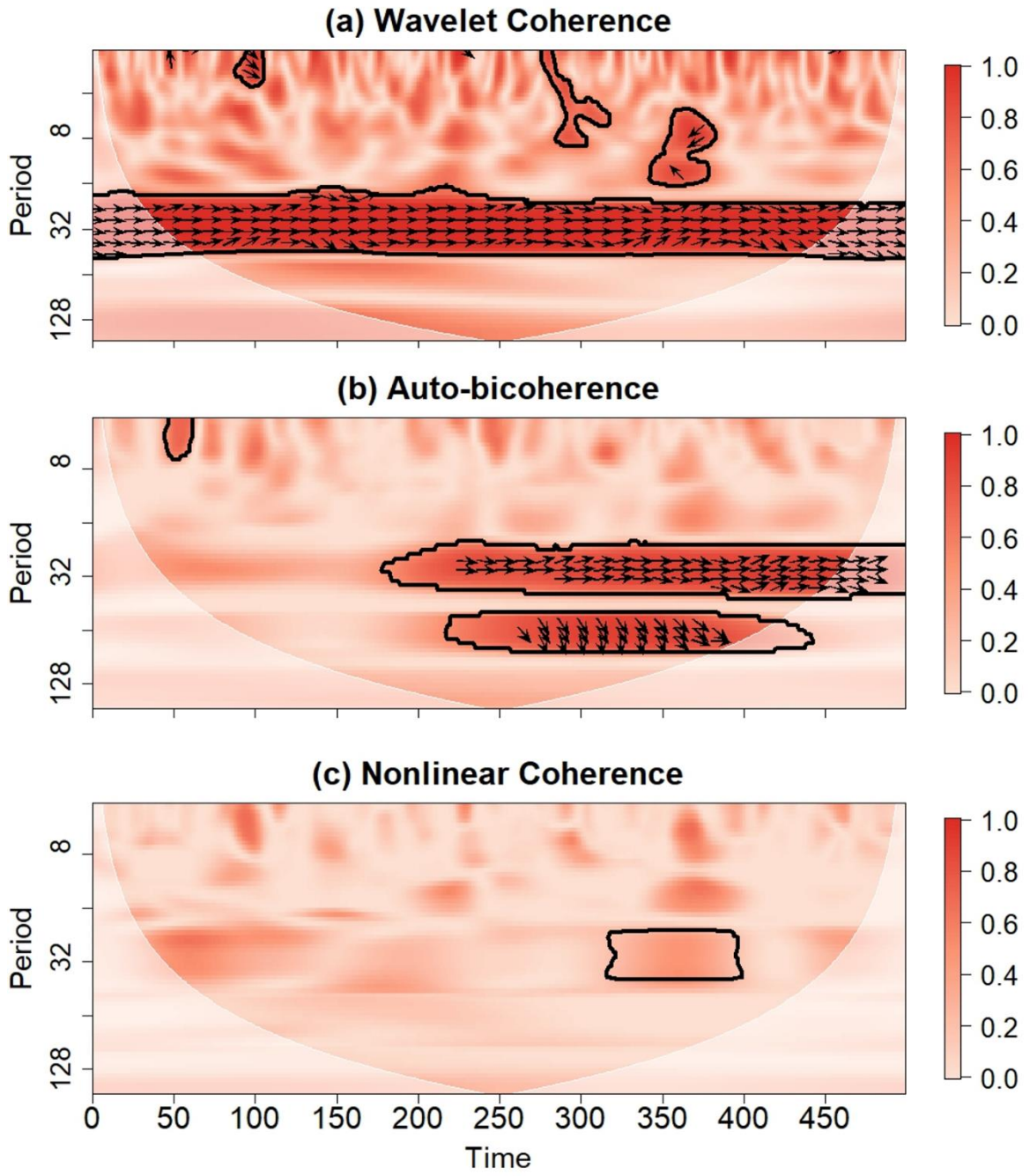

Figure 2. (a) Wavelet coherence between the time series of $F(t)$ and $R(t)$ shown in Figure 1. Arrows indicate the relative phase difference, where arrows pointing to the right mean that the time series are in phase. (b) The local diagonal slice of the auto-bicoherence spectrum of $F(t)$. Arrows represent the bi-phase, where arrows pointing to the right mean that the phase coupling between the mode with period indicated on the vertical axis and its harmonic contributes to positive skewness. (c) Nonlinear coherence between $F(t)$ and $R(t)$. Contours in all panels enclose regions of 5% cumulative area-wise significance. Light-shaded region represents the cone of influence where edge effects may be important.

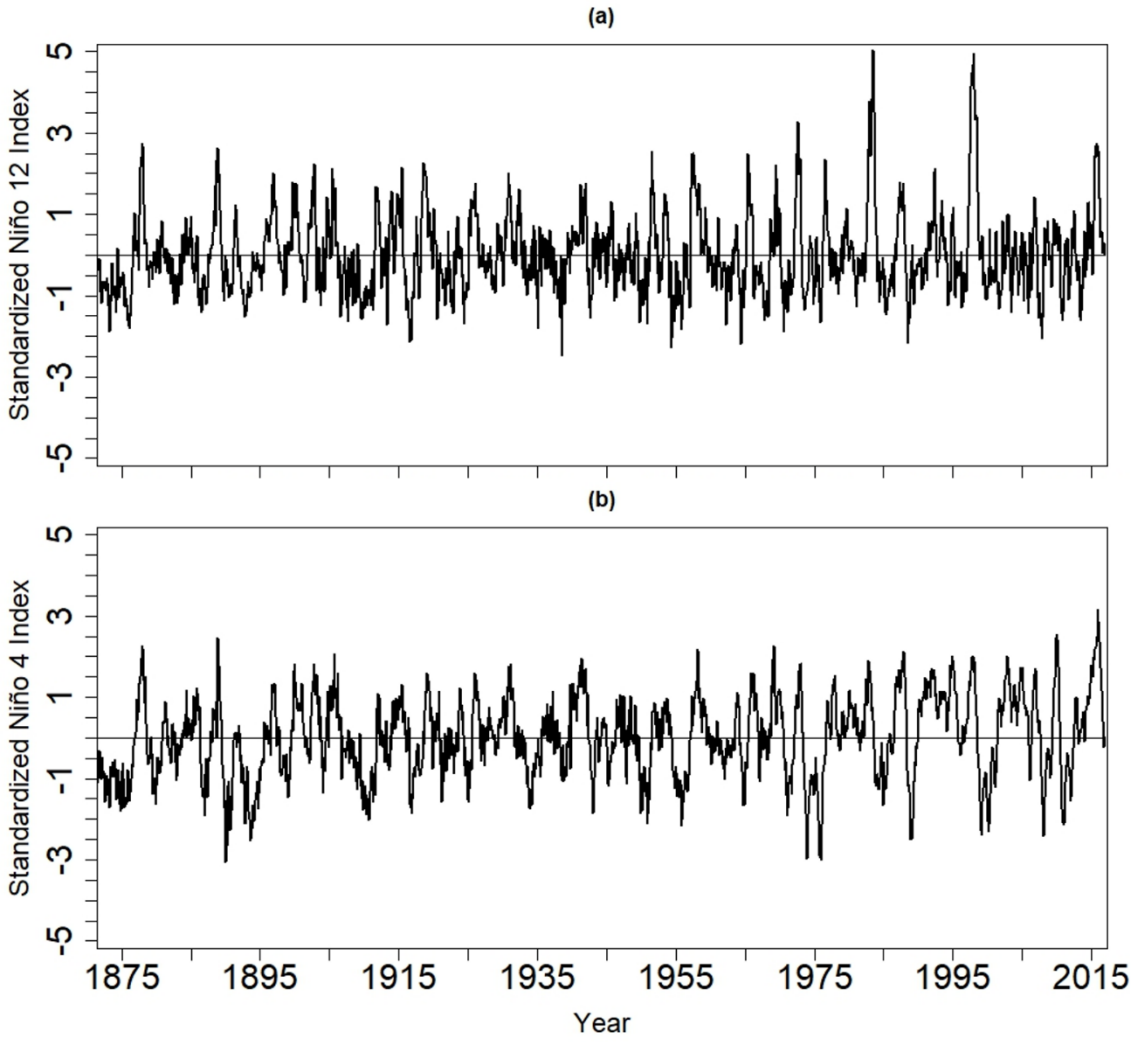

1343

1344 Figure 3. The ~~(a)~~ time series of the ~~and (b) event spectrum of the~~ (a) Niño 1+2 and (b) ~~index.~~indices.

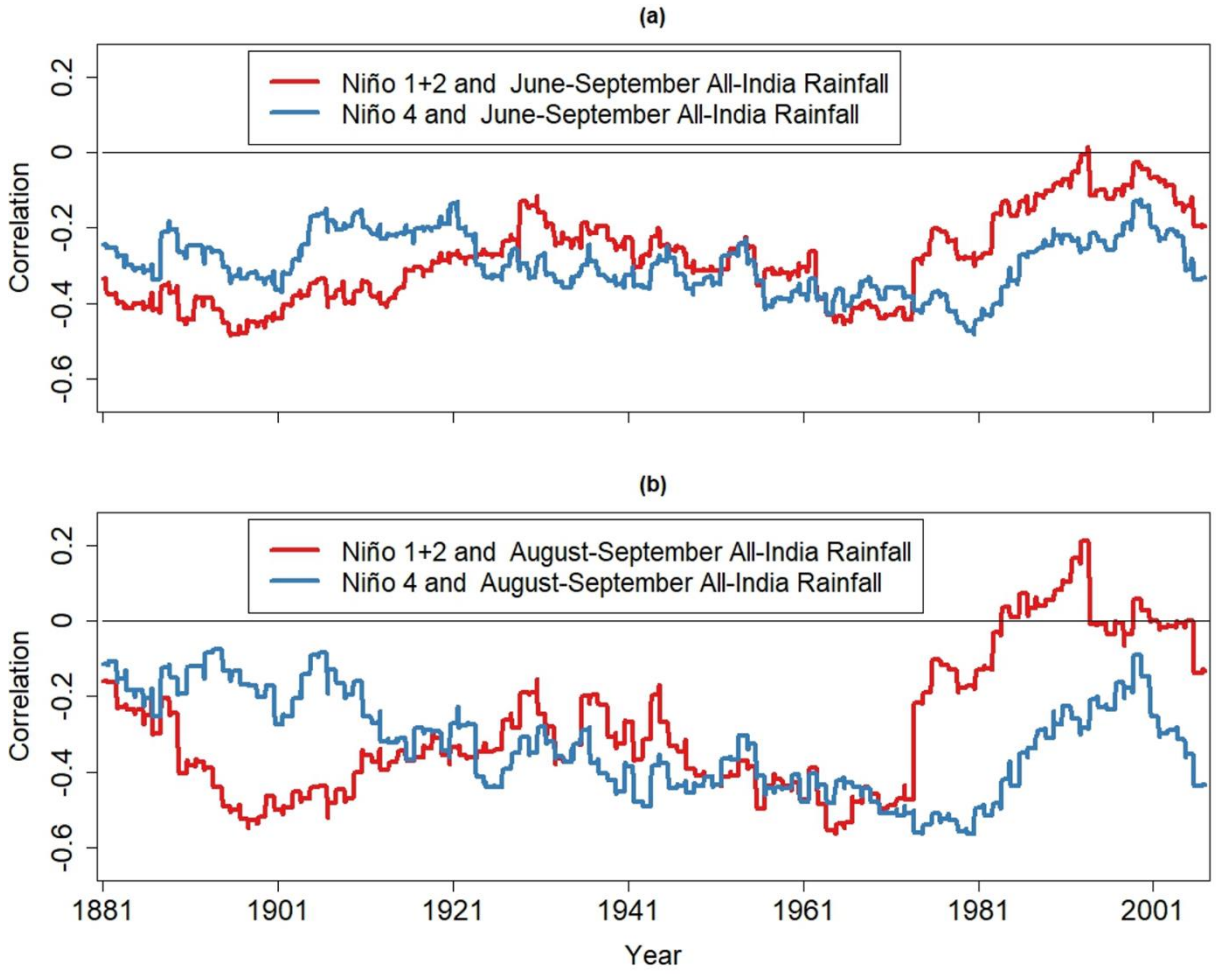

Figure 4 ~~Figure 5. 20-year sliding skewness of June-September All-India rainfall and time series for the Niño 1+2 and Niño 4 indices.~~ (b) 20-year sliding correlation between anomalies for June-September All-India rainfall and the time series for the Niño 1+2 and Niño 4 indices. (c) Same as (b) but for August-September All-India rainfall.

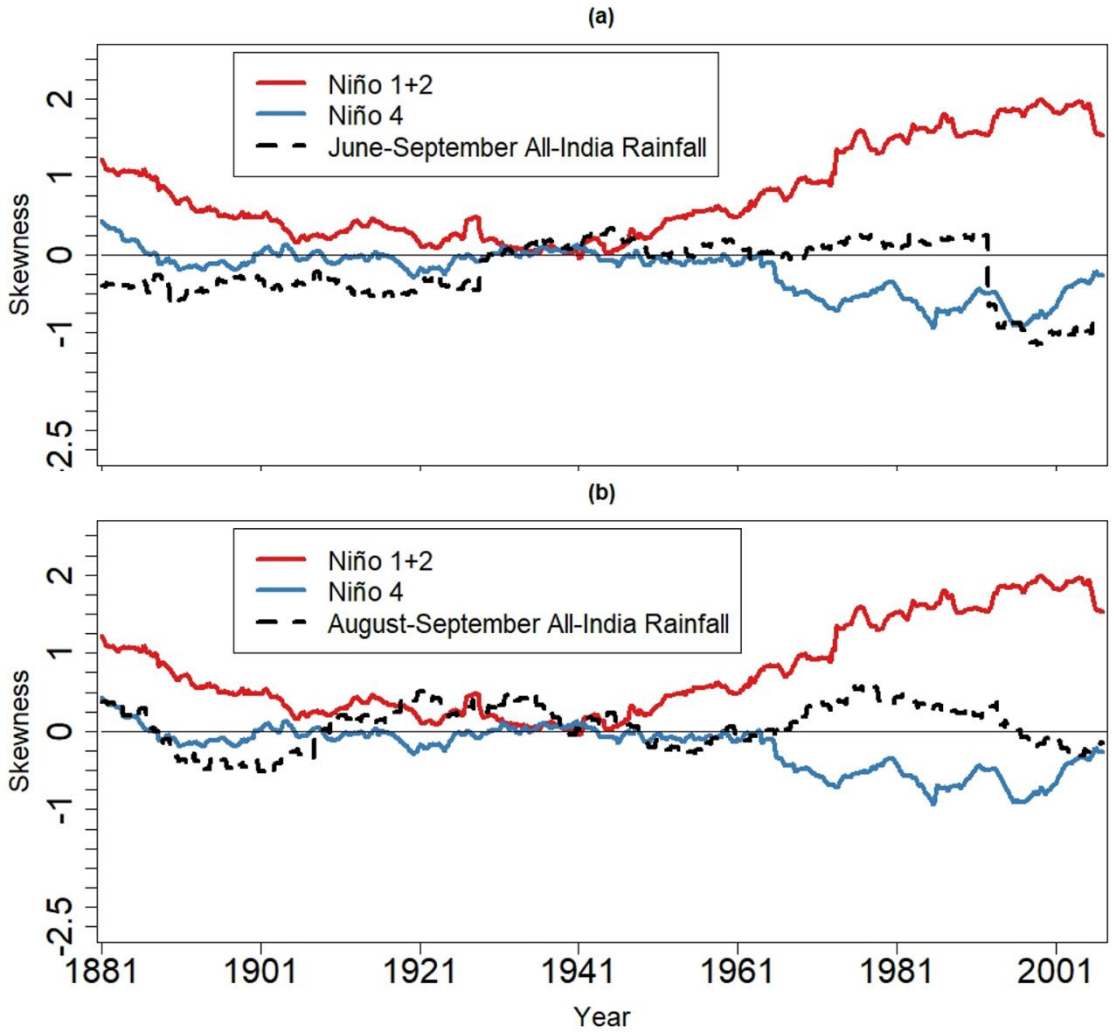

Figure 5. 20-year sliding skewness of (a) June-September and (b) August-September All-India rainfall and time series for the Niño 1+2 and Niño 4 indices.

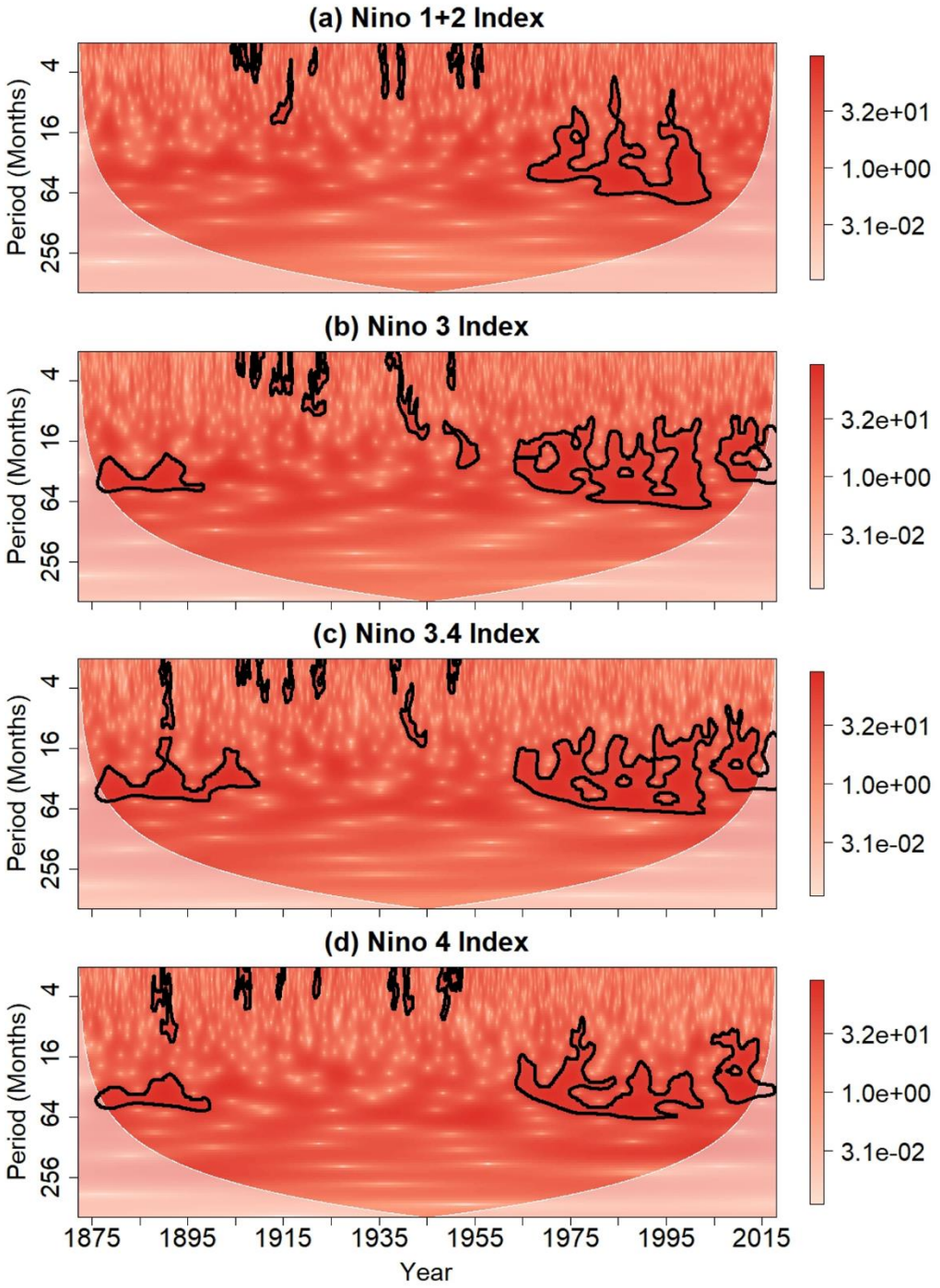

Figure 6. Wavelet Power spectrum of the (a) Niño 1+2, (b) Niño 3, (c) Niño 3.4, and (d) Niño 4 indices. Contours enclose regions of 5% cumulative area-wise significance. Light-shaded region represents the cone of influence, which is the region where edge effects are non-negligible.

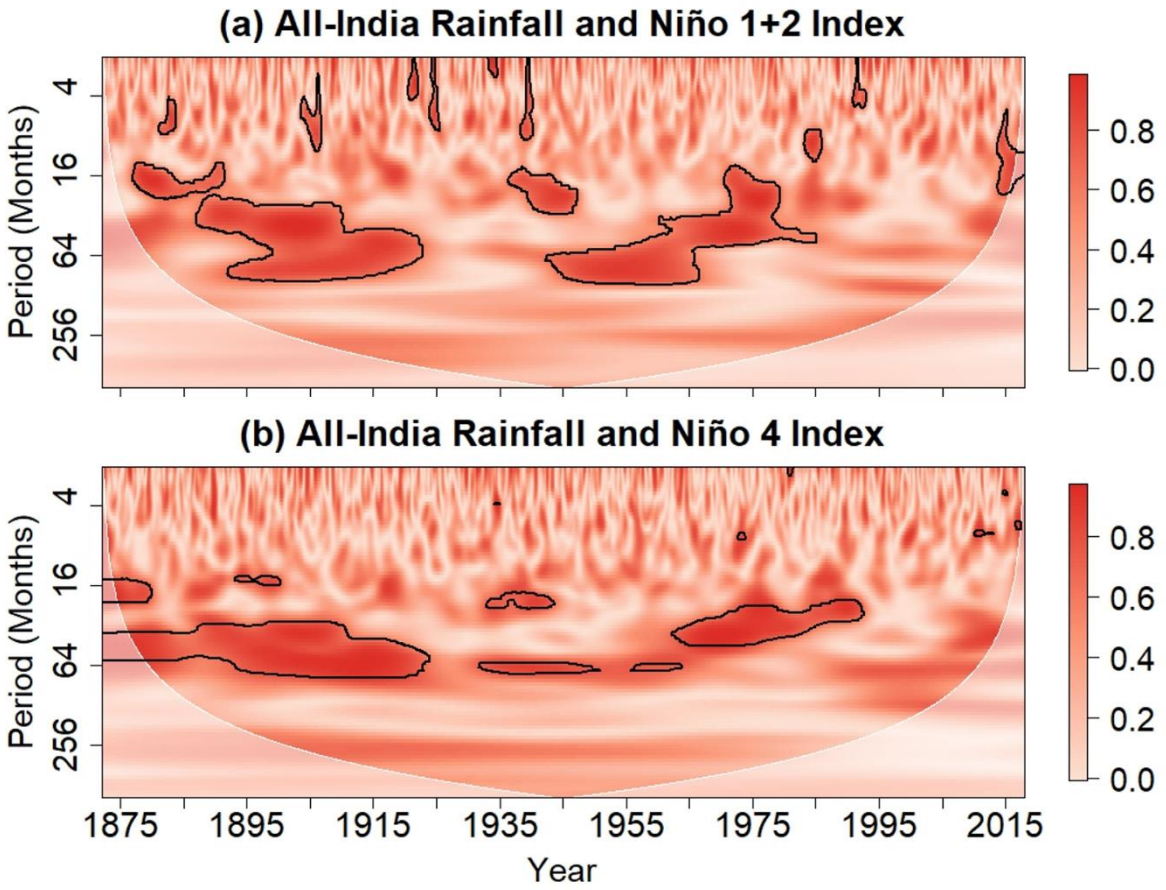

Figure 7. Wavelet coherence spectrum between All-India rainfall anomalies and time series for the (a) Niño 1+2 and (b) Niño 4 indices. Contours enclose regions of 5% cumulative area-wise significance. Light-shaded region represents the cone of influence, which is the region where edge effects are non-negligible.

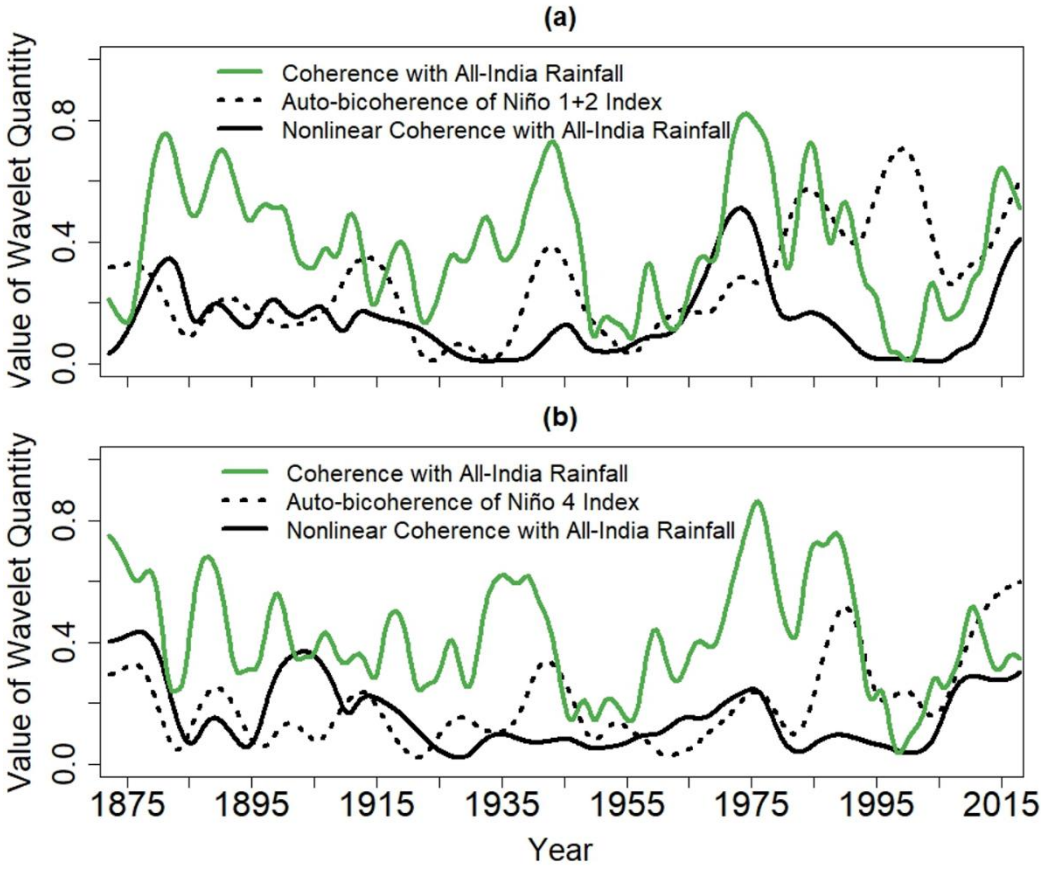

Figure 8. (a) The wavelet coherence between All-India rainfall and the Niño 1+ 2 index, the auto-bicoherence of the Niño 1+2 index, and the nonlinear coherence between the Niño 1+2 index and All-India rainfall anomalies averaged in the period band of 16 to 64 months. (b) The same as (a) but with the Niño 4 index.

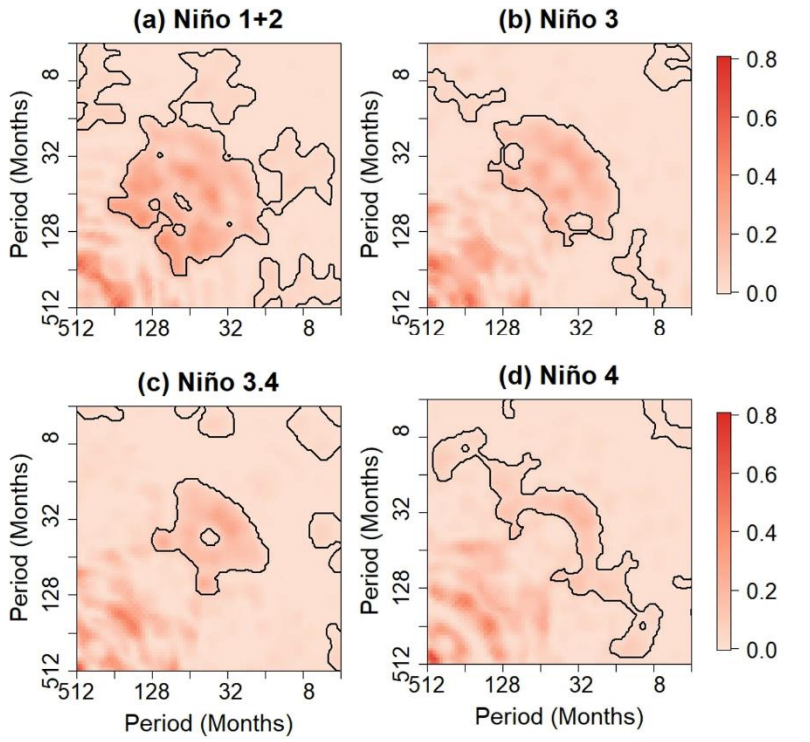

Figure 9. Global auto-bicoherence spectra of the (a) Niño 1+2, (b) Niño 3, (c) Niño 3.4, and (d) Niño 4 indices. Contours enclose regions of 5% cumulative area-wise significance.

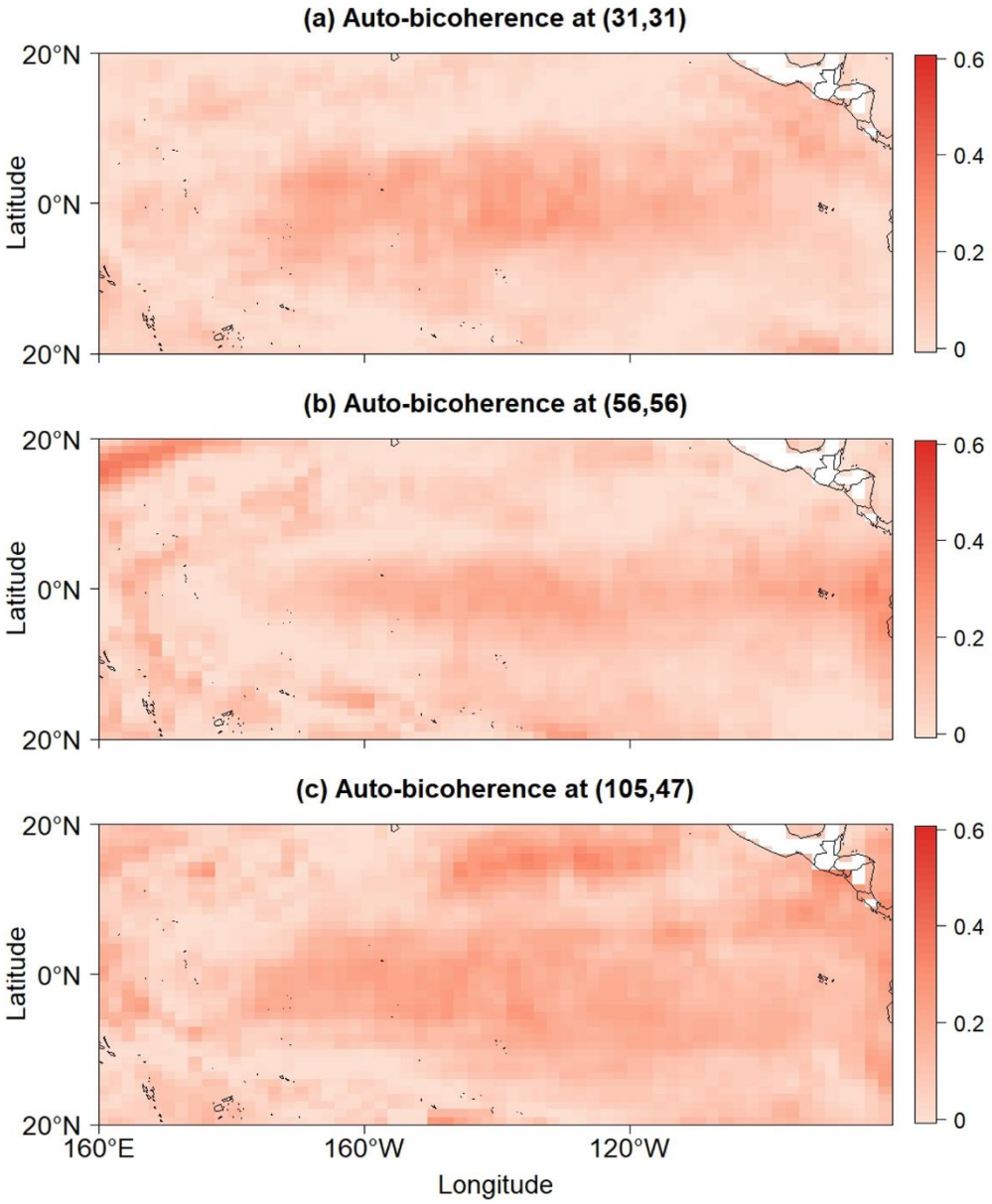

Figure 10. Global auto-bicoherence corresponding to the pairs (a) (31, 31), (b) (56, 56), and (c) (105, 47) [months].

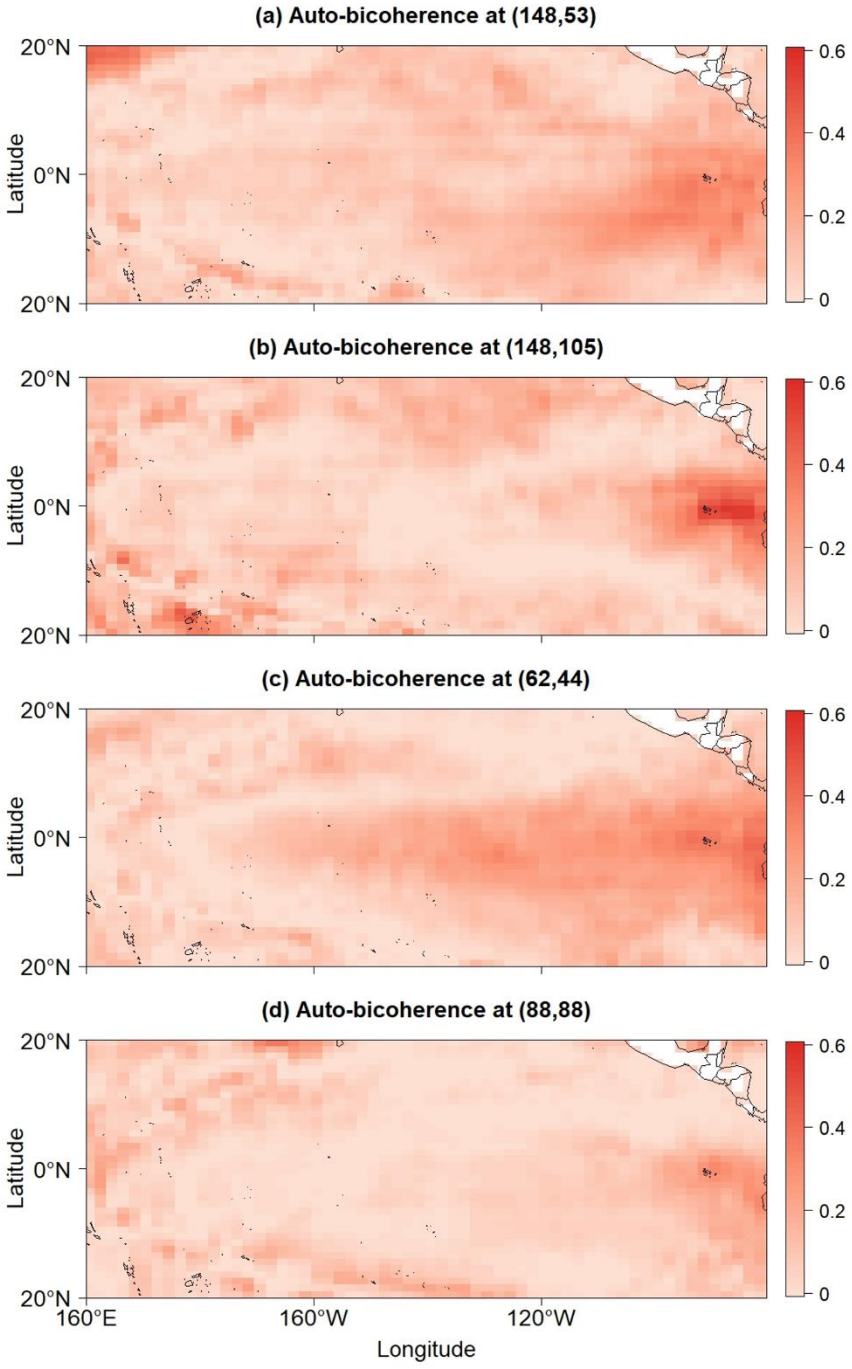

Figure 11. Global auto-bicoherence corresponding to the pairs (a) (158, 43), (b) (148, 105), (c) (62, 44), and (d) (88,88) [months].

Figure 12. Global auto-bicoherence spectra of the (a) All-India, (b) Peninsula, (c) Northwest, (d) Northeast, (e) West Central, and (f) Central Northeast time series. Contours enclose regions of 5% cumulative area-wise significance.

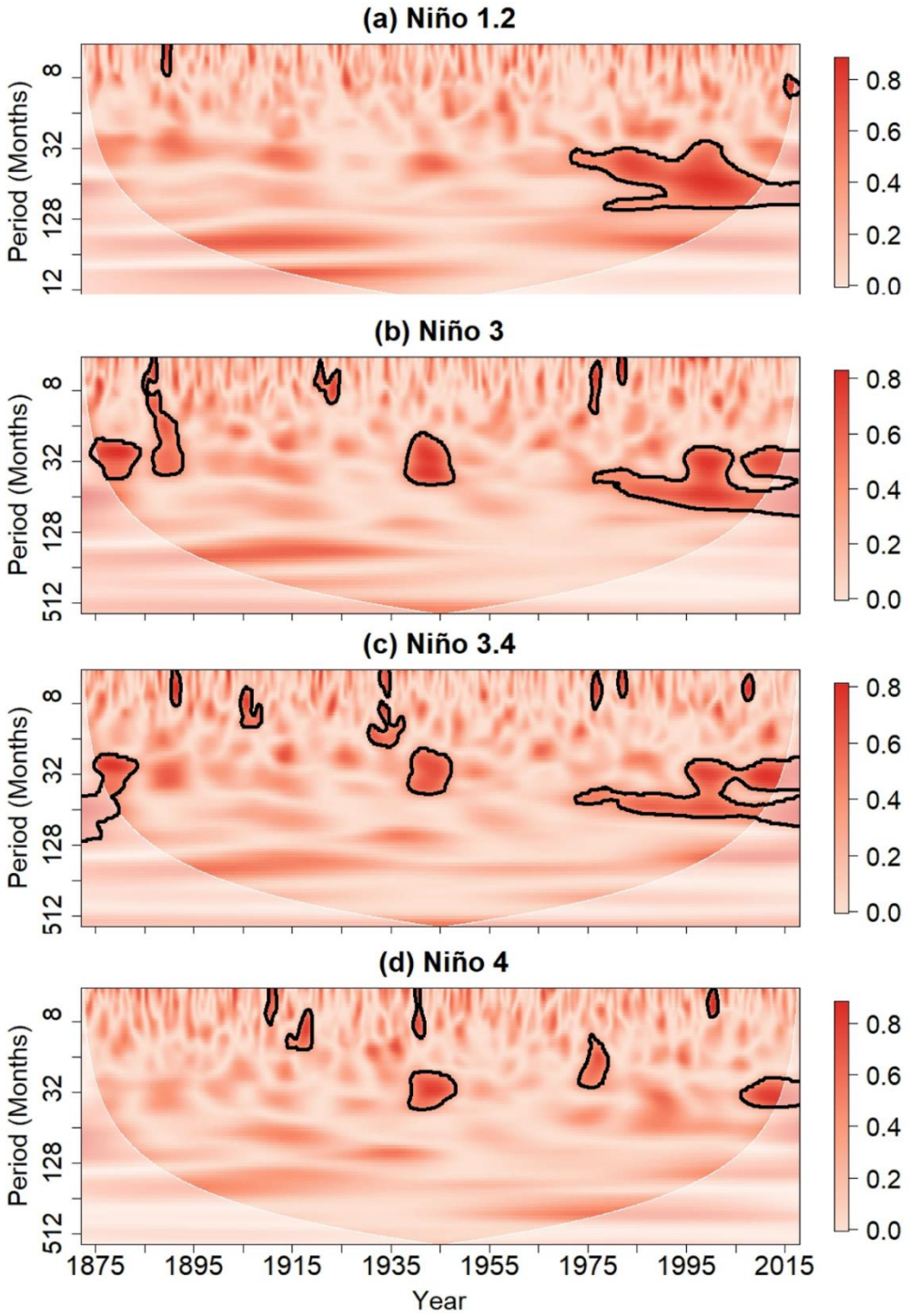

Figure 13. Local auto-bicoherence spectra of the (a) Niño 1+2, (b) Niño 3, (c) Niño 3.4, and (d) Niño 4 indices. Contours enclose regions of 5% cumulative area-wise significance and the light shading represents the cone of influence.

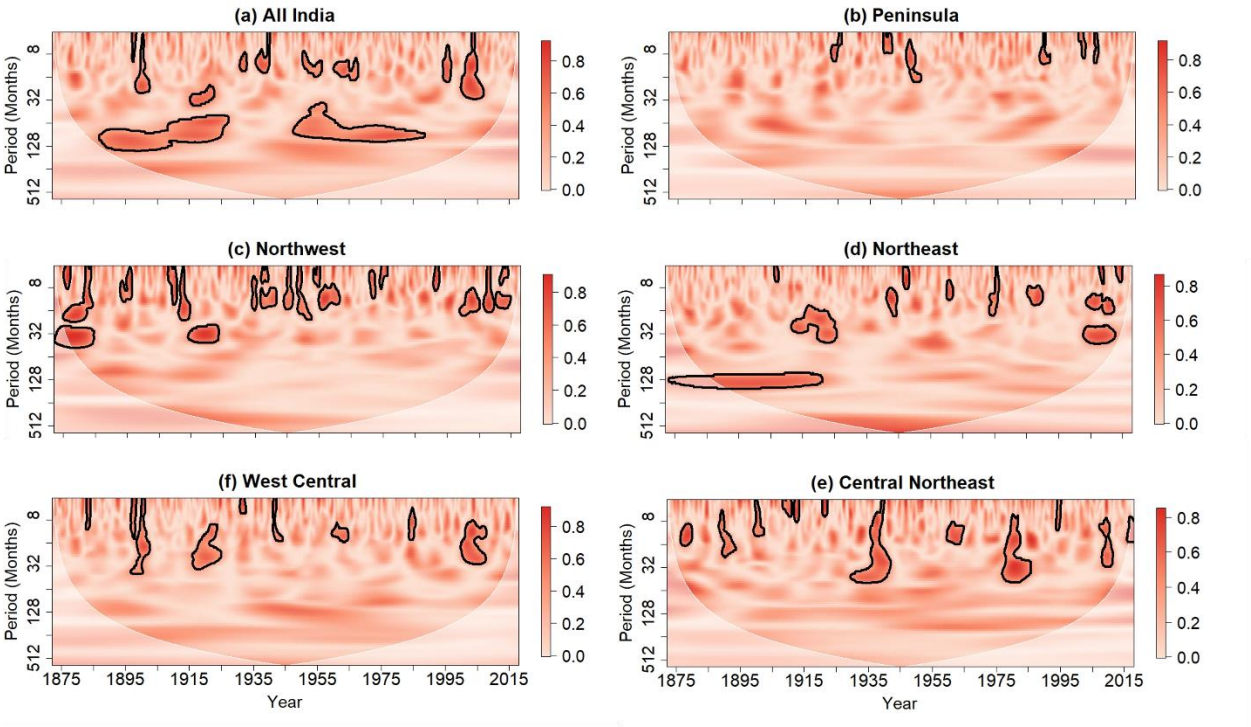

Figure 14. Local auto-bicoherence spectra of the (a) All-India, (b) Peninsula, (c) Northwest, (d) Northeast, (e) West Central, and (f) Central Northeast time series. Contours enclose regions of the 5% cumulative area-wise significance and the light shading represents the cone of influence.

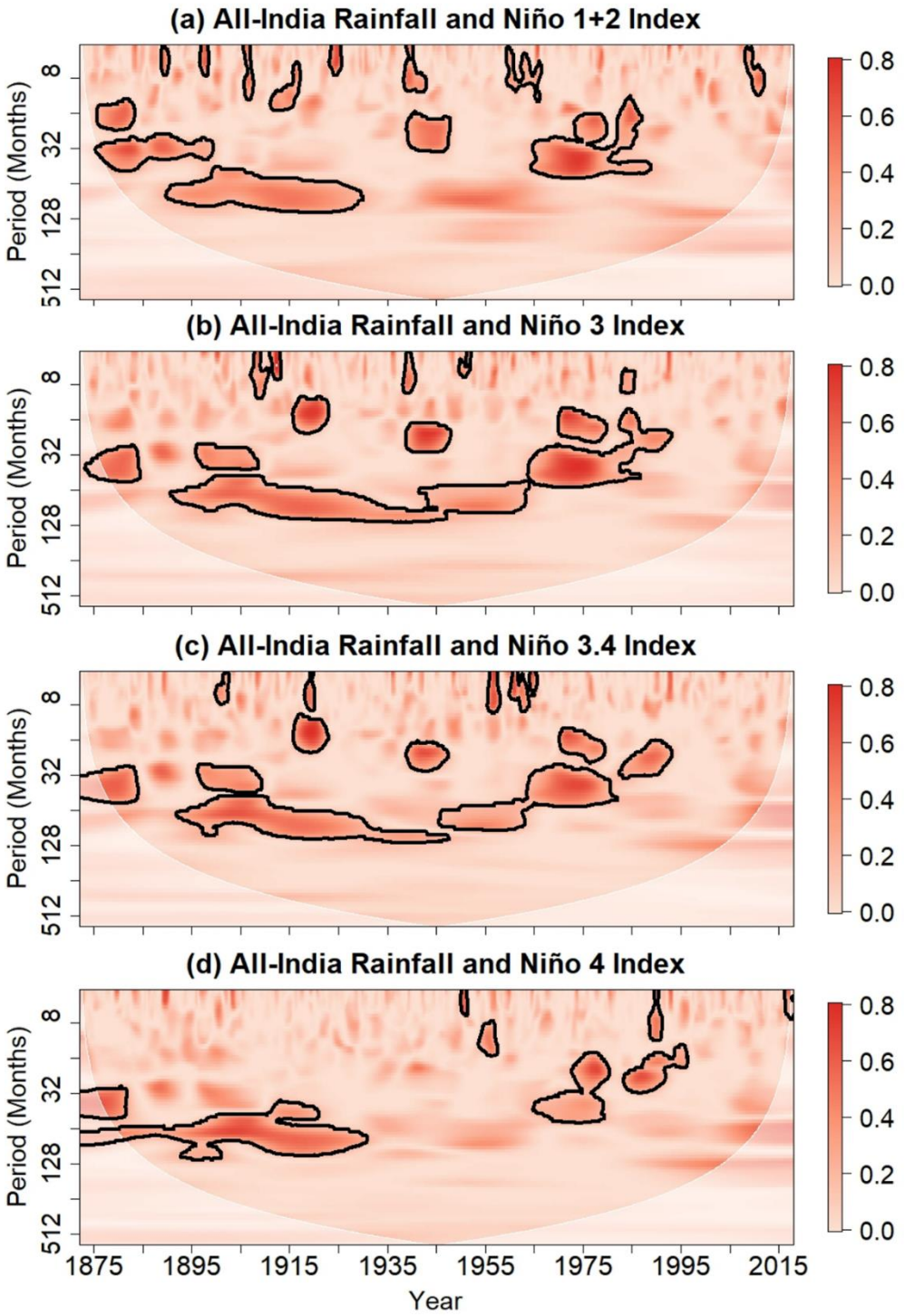

Figure 15. Nonlinear wavelet coherence between the All-India time series and times series for the (a) Niño 1+2, (b) Niño 3, (c) Niño 3.4, and (d) Niño 4 indices. Contours enclose regions of 5% cumulative area-wise significance and light shading represents the cone of influence.

Table 1. Wavelet quantities and what they measure.

Linear Coherene	Measures the correlation between two time series at a particular time scale.
Global Auto-bicoherence	Measures the time-averaged
Local Auto-bicoherence	Measures the degree of nonlinear
Nonlinear Coherence	Measures the cross-correlation between nonlinear modes